

1 **Beyond accessibility: ATAC-seq footprinting unravels kinetics**
2 **of transcription factor binding during zygotic genome**
3 **activation**

4 **Authors**

5 Mette Bentsen¹, Philipp Goymann¹, Hendrik Schultheis¹, Anastasiia Petrova¹, Kathrin Klee¹,
6 Annika Fust¹, Jens Preussner^{1,3}, Carsten Kuenne¹, Thomas Braun^{2,3}, Johnny Kim^{2,3}, Mario
7 Looso^{1,3}

8

9 **Affiliation**

10 ¹ Bioinformatics Core Unit (BCU), Max Planck Institute for Heart and Lung Research, Bad
11 Nauheim, Germany

12 ² Department of Cardiac Development and Remodeling, Max-Planck-Institute for Heart and
13 Lung Research, Bad Nauheim, Germany

14 ³ German Centre for Cardiovascular Research (DZHK), Partner site Rhein-Main, Frankfurt am
15 Main, 60596 Germany

16

17 **Corresponding author email address**

18 mario.looso@mpi-bn.mpg.de, @loosolab

19 **Abstract**

20 While footprinting analysis of ATAC-seq data can theoretically enable investigation of
21 transcription factor (TF) binding, the lack of a computational method implementing both
22 footprinting, visualization and downstream analysis has hindered the widespread application
23 of this method. Here we present TOBIAS, a comprehensive footprinting framework enabling
24 genome-wide investigation of TF binding dynamics for hundreds of TF simultaneously. As a
25 proof-of-concept, we illustrate how TOBIAS can unveil complex TF dynamics during zygotic
26 genome activation (ZGA) in both humans and mice, and explore how the TF Dux activates
27 cascades of TF, binds to repeat elements and induces expression of novel genetic elements.
28 TOBIAS is freely available at: <https://github.com/loosolab/TOBIAS>.

29

30 **Keywords**

31 Footprinting, ATAC-seq, epigenetics, transcription factors, ZGA, Dux

32

33 **Background**

34 Epigenetic mechanisms governing chromatin organization and transcription factor (TF)
35 binding are critical components of transcriptional regulation and cellular transitions. In recent
36 years, rapid improvements of pioneering sequencing methods such as ATAC-seq (Assay of
37 Transposase Accessible Chromatin) [1], have allowed for systematic, global scale
38 investigation of epigenetic mechanisms controlling gene expression. While ATAC-seq can
39 uncover accessible regions where TFs might bind, true identification of specific TF binding
40 sites (TFBS) still relies on chromatin immunoprecipitation methods such as ChIP-seq.
41 However, ChIP-seq methods require high input cell numbers, are limited to one TF per assay,
42 and are further restricted to TFs for which antibodies are readily available. Latest
43 improvements of ChIP based methods [2] can circumvent some of these technical drawbacks,
44 but the limitation of only being able to identify binding sites of one TF per assay persists.
45 Therefore, it remains costly, or even impossible, to study the binding of multiple TFs in parallel.

46 The limitations of investigating TF binding become particularly apparent when investigating
47 processes involving a very limited number of cells such as preimplantation development (PD)
48 of early zygotes. PD encompasses the transformation of the fertilized egg that forms the
49 zygote, which subsequently undergoes a series of cell divisions to finally constitute the
50 blastocyst, a structure built by the inner cell mass (ICM) and trophectoderm (Figure 1a).
51 Following fertilization, maternal and paternal mRNAs are degraded prior to zygotic genome
52 activation (ZGA) (reviewed in [3]), which leads to the transcription of thousands of genes [4].
53 Integration of multiple omics-based profiling methods have revealed a set of key TFs that are
54 expressed at the onset of and during ZGA including Dux [5, 6], Zscan4 [7], and other
55 homeobox-containing TFs [8]. However, what genetic elements they directly bind to and/or
56 regulate during PD remains poorly understood. Consequently, the global network of TF
57 binding dynamics throughout PD remains almost entirely obscure.

58 A computational method known as *digital genomic footprinting* (DGF) [9] has emerged as an
59 alternative means, which can overcome some limitations of investigating TF binding with ChIP-
60 based methods. DGF is a computational analysis of chromatin accessibility assays such as
61 ATAC-seq, which makes use of the intrinsic effect that DNA effector enzymes only cut
62 accessible DNA regions. Similarly to nucleosomes, bound TFs hinder cleavage of DNA,
63 resulting in defined regions of decreased signal strength within larger regions of high signal -
64 known as *footprints* [10] (Figure 1b). This concept shows considerable potential as it
65 theoretically allows to survey genome-wide binding of multiple TFs in parallel from a single
66 experiment.

67 However, there are still a multitude of challenges to DGF methods [11, 12]. While ATAC-seq
68 became very popular as it is simpler and require less starting material in comparison to
69 DNase-seq, only a few of the existing footprinting tools inherently support ATAC-seq analyses
70 [13-16]. In this context the non-random behavior of cleavage enzymes that bind preferentially
71 to certain sequence compositions (e.g. Tn5 bias for ATAC-seq) turned out to be a major
72 challenge [17-20]. In addition, computational issues such as software availability, the use of
73 non-standard file-formats, varying dependencies and lack of support for multiprocessing have
74 made current footprinting tools hard to integrate into existing analysis pipelines. Aside from
75 the identification of footprints, the challenge of integrating footprints, TF motifs and genomic
76 location of genes to be able to fully investigate the epigenetic processes involving TF binding
77 is not a trivial task.

78 While all of these factors significantly influence the outcome of footprinting analyses, previous
79 investigations have been focused on improving individual computational steps such as
80 estimating differential TF binding on a global scale [21-23], identifying footprints for specific
81 TFs in a local genomic context [16, 24], or correcting the bias within the genomic signals [25,
82 26]. Few methods have included bias correction as an integrated part of footprint detection
83 [16]. Essentially, a comprehensive framework that takes all of these parameters into account
84 does not exist.

85 Here we describe and exploit application of TOBIAS (Transcription factor Occupancy
86 prediction By Investigation of ATAC-seq Signal), a comprehensive computational framework
87 that we created for footprinting analysis (Figure 1c). TOBIAS is a collection of computational
88 tools utilizing a minimal input of ATAC-seq reads (.bam-format), TF motif information (in the
89 form of PWMs) and genome information to enable Tn5 bias correction, footprinting, and
90 comparison of TF binding even for complex experimental designs (e.g. time series).
91 Furthermore, TOBIAS includes a variety of modules for downstream analysis such as TF
92 network inference and visualization of footprints. In addition to the TOBIAS Python package,
93 we provide scalable analysis workflows implemented in Snakemake [27] and NextFlow [28],
94 including a cloud computing compatible version making use of the de.NBI cloud [29].

95 **Results**

96 **Validation of TOBIAS**

97 As a comprehensive framework for DGF analysis comparable to TOBIAS does not exist, we
98 rated the individual TOBIAS modules in a well-studied system of paired ATAC-seq and ChIP-
99 seq datasets (see Methods; Validation) against published methods where possible. In terms
100 of Tn5 bias correction, we found that TOBIAS outperforms other tools in distinguishing
101 between bound/unbound sites (Supp. Figure 1a, Supp. File 1). For detection of footprints, we
102 also found that TOBIAS clearly outperforms other known methods capable of screening TFs
103 in parallel (Supp. Figure 1b left and methods). By making use of another exemplary dataset
104 of ATAC-seq data derived from hESC [30], we confirmed the obvious improvement of footprint
105 detection after Tn5 bias correction (Supp. Figure 2a left). Importantly, we also identified a
106 number of cases where the TF motif itself is a disfavored position for Tn5 integration, thereby
107 creating a false-positive footprint if left uncorrected, which disappears after Tn5 bias correction
108 (Supp. Figure 2a; right). Utilizing a footprint metric as described by [22] (Supp. Figure 2b)
109 across different stages of Tn5 bias correction (uncorrected/expected/corrected signals), we
110 found a high correlation between uncorrected and expected footprinting depths (Supp. Figure

111 2c). In contrast, this effect vanished after TOBIAS correction (Supp. Figure 2d), indicating the
112 gain of a real footprint information superimposed by Tn5 bias. In a global perspective, taking
113 590 TFs into account, TOBIAS generated a measurable footprint for 64% of the TFs (Supp.
114 Figure 2e). This is in contrast to previous reports wherein it has been suggested that only 20%
115 of all TFs leave measurable footprints [22]. To summarize, we found that TOBIAS exceeded
116 other software solutions in terms of correctly identifying bound TF binding sites.

117

118 **Footprinting uncovers transcription factor binding dynamics in mammalian ZGA**

119 To demonstrate the full potential of TOBIAS, in particular in the investigation of processes
120 involving only few cells, we analyzed a series of ATAC-seq datasets derived from both human
121 and murine preimplantation embryos at different developmental stages ranging from 2C, 4C,
122 8C to ICM in addition to embryonic stem cells of their respective species [30] [31]. Altogether,
123 TOBIAS was used to calculate footprint scores for a list of 590 and 464 individual TFs across
124 the entire process of PD of human and mouse embryos, respectively. After clustering TFs into
125 co-active groups within one or multiple developmental timepoints (Human: Figure 2a and
126 Supp. Table 1; Mouse: see next section), we first asked whether the predicted timing of TF
127 activation reflects known processes in human PD. Intriguingly, we found 10 defined clusters
128 of specific binding patterns, the majority of which peaked between 4C and 8C, fully concordant
129 with the transcriptional burst and termination of ZGA (Figure 2a).

130 Two clusters of TFs (Cluster 1+2; n=83) displayed highest activity at the 2-4C stage and
131 strongly decreased thereafter, suggesting that factors within these clusters are likely involved
132 in ZGA initiation. We set out to classify these TFs, and observed a high overlap with known
133 maternally transferred transcripts [32] (LHX8, BACH1, EBF1, LHX2, EMX1, MIXL1, HIC2,
134 FIGLA, SALL4, ZNF449), explaining their activity before ZGA onset. Importantly, DUX4 and
135 DUXA, which are amongst the earliest expressed genes during ZGA [5, 6], were also
136 contained in these clusters. Additional TFs included HOXD1, which is known to be expressed
137 in human unfertilized oocytes and preimplantation embryos [33] and ZBTB17, a TF mandatory

138 to generate viable embryos [34]. Cluster 6 (n=67) displayed a particularly prominent 8C
139 specific signature, that harbored well known TFs involved in lineage specification such as
140 PITX1, PITX3, SOX8, MEF2A, MEF2D, OTX2, PAX5 and NKX3.2. Furthermore, overlapping
141 TFs within Cluster 6 with RNA expression datasets ranging from the germinal vesicle to
142 cleavage stage [5], 12 additional TFs (FOXJ3, HNF1A, ARID5A, RARB, HOXD8, TBP, ZFP28,
143 ARID3B, ZNF136, IRF6, ARGFX, MYC, ZSCAN4) were confirmed to be exclusively expressed
144 within this time frame. Taken together, these data show that TOBIAS reliably uncovers
145 massively parallel TF binding dynamics at specific time points during early embryonic
146 development.

147

148

149

150 **Transcription factor scores correlate with footprints and gene expression**

151 To confirm that TOBIAS-based footprinting scores are indeed associated with leaving *bona*
152 *fide* footprints we utilized the ability to visualize aggregated footprint plots as implemented
153 within the framework. Indeed, bias corrected footprint scores were highly congruent with
154 explicitly defined footprints (Figure 2b) of prime ZGA regulators at developmental stages in
155 which these have been shown to be active [7]. For example, footprints associated with DUX4,
156 a master inducer of ZGA, were clearly visible from 2C-4C, decreased from 8C onwards and
157 were completely lost in later stages, consistent with known expression levels [30] and ZGA
158 onset in humans. Footprints for ZSCAN4, a primary DUX4 target [5], were exclusively visible
159 at the 8C stage. Interestingly, GATA2 footprints were exhibited from 8C to ICM stages which
160 is in line with its known function in regulating trophoblast differentiation [35]. As expected,
161 CTCF creates footprints across all timepoints. Strikingly, we observed that these defined
162 footprints were not detectable without TOBIAS mediated Tn5 bias correction (Supp. Figure
163 2f). These data show that footprint scores can be reliably confirmed by footprint visualizations,
164 which further allow to infer TF binding dynamics.

165 To test if the global footprinting scores of individual TFs correlate with the incidence and level
166 of their RNA expression, we matched them to RNA expression datasets derived from
167 individual timepoints throughout zygotic development, taking TF motif similarity into account.
168 Indeed, we found that TOBIAS scores for the majority of TFs either correlated well with the
169 timing of their expression profiles or displayed a slightly delayed activity after expression
170 peaked (Supp. Figure 3a). This is important because it shows that in conjunction with
171 expression data, TOBIAS can unravel the kinetics between TF expression (mRNA) and the
172 actual binding activity of their translated proteins. The value of this added information becomes
173 particularly apparent when analyzing activities of TFs that did not correlate with the timing of
174 their RNA expression (Supp. Figure 3a; not correlated).

175 For example, within the non-correlated cluster 13 TFs were identified which are of putative
176 maternal origin [32] including SALL4. In mice, Sall4 protein is maternally contributed to the
177 zygote, subsequently degraded at 2C and then reexpressed after zygotic transcription has
178 initiated [36]. Consistent with this, SALL4 expression increased dramatically from 8C onwards
179 (Supp. Table 2). Notably, TOBIAS predicted SALL4 to have the highest activity in 2C and
180 second-highest activity in hESC (on-off-on-pattern). These data show that TOBIAS can predict
181 true on-off-on-patterns, and can infer significant insight into TF activities, in particular for those
182 where determining their expression patterns alone does not suffice to explain when they exert
183 their biological function.

184

185 **Differential footprint analysis reveals functional divergence between human and mouse**

186 **ZGA**

187 The timing of ZGA varies between mice (2C) and humans (4C to 8C) (reviewed in [37] [38]).
188 By integrating the TOBIAS scores from human and mouse (Supp. Figure 3b and Supp. Table
189 3), and instrumentalizing the capability of TOBIAS to generate differential TF binding plots for
190 all time points automatically, we investigated similarities and differences of PD between these
191 species. Firstly, reflecting the shift of ZGA onset, we identified 30 TFs which appeared to be

192 ZGA specific in both human and mouse (Figure 2c) including several homeobox factors which
193 already have described functions within ZGA [39] as well as ARID3A which has been shown
194 to play a role in cell fate decisions in creating trophectoderm [40].

195 Next, we used the differential TF binding plots to display differences in ZGA at the transition
196 between 2C and 4C in mouse (Figure 3a), and human 8C and ICM (Figure 3b) (Supp. File 2
197 + 3 for all pairwise comparisons). In mice, we observed a shift of Obox-factor activity in 2C to
198 an activation of Tead (Tead1-4) and AP-2 (Tfap2a/c/e) motifs in 4C. Notably, AP2/Tfap2c is
199 required for normal embryogenesis in mice [41] and was also recently shown to act as a
200 chromatin modifier that opens enhancers proximal to pluripotency factors in human [42]. We
201 observed a similar shift of TF activity for homeobox factors such as PITX1-3, RHOXF1, CRX
202 and DMBX1 at the human 8C stage towards higher scores in ICM for known pluripotency
203 factors such as POU5F1 (OCT4) and other POU-factors. Taken together, these results
204 highlight the ability of TOBIAS to capture differentially bound TFs, not only across the whole
205 timeline, but also between individual conditions and species.

206 Throughout the pairwise comparisons, we observed that TFs from the same families often
207 display similar binding kinetics within species, which is not surprising since they often possess
208 highly similar binding motifs (Figure 3a right). To characterize TF similarity, TOBIAS provides
209 functionality to cluster TFs based on the overlap of TFBS within investigated samples (Figure
210 3c+3d). This enables quantification of the similarity and clustering of individual TFs that appear
211 to be active at the same time. Thereby, we observed a group of homeobox motifs which cluster
212 together with more than 50% overlap of their respective binding sites in mouse (Figure 3c). In
213 contrast, other TFs such as Tead and AP-2 cluster separately, indicating that these factors
214 utilize independent motifs (Supp. File 2+3). While this might appear trivial, this clustering of
215 TFs in fact also highlights differences in motif usage between human and mouse. One
216 prominent example is the RHOXF1 motif, which shows high binding-site overlap with Obox
217 1/3/5 and Otx2 binding sites in mouse (Figure 3c; ~60% overlap), but does not cluster with
218 OTX2 in human (Figure 3d; ~35% overlap). This observation suggests important functional

219 differences of RHOX/Rhox TFs between mice and humans. In support of this hypothesis
220 RHOXF1, RHOXF2 and RHOXF2B genes are exclusively expressed at 8C and ICM in
221 humans, whereas Rhox factors are not expressed in corresponding developmental stages of
222 preimplantation in mouse (Supp. Table 4). Conceivably, this observation, together with the
223 finding that murine Obox factors share the same motif as RHOX-factors in humans, suggests
224 that Obox TFs might function similarly to RHOX-factors during ZGA. Altogether, the TOBIAS
225 mediated TF clustering based on TFBS overlap allows for quantification of target-similarity
226 and divergence of TF function between motif families.

227

228 **Dux expression induces massive changes of chromatin accessibility, transcription and** 229 **TF networks**

230 We became particularly attracted to Dux/DUX4 which TOBIAS correctly predicted to be one
231 of the earliest factors to be active in both human and mouse (Figure 2a and Supp. Figure
232 3b)[5-7, 43, 44]. Despite its prominent role in ZGA, there is however still a poor understanding
233 of how Dux regulates its primary downstream targets, and consequently its secondary targets,
234 during this process. We therefore applied TOBIAS to identify Dux binding sites utilizing an
235 ATAC-seq dataset of Dux overexpression (DuxOE) in mESC [5].

236 Inspecting the differential TF activity predicted by TOBIAS, we observed an increase of activity
237 of Dux, Obox and other homeobox-TFs as expected (Figure 4a, Supp. File 4). Interestingly,
238 this went along with a massive loss of TF binding for pluripotency markers such as Nanog,
239 Pou5f1 (OCT4) and Sox2 upon DuxOE, indicating that Dux renders previously accessible
240 chromatin sites associated with pluripotency inaccessible.

241 Consistently, Dux footprints (Figure 4b; left) were clearly evident upon DuxOE. Importantly,
242 TOBIAS discriminated ~30% of all potential binding sites within open chromatin regions to be
243 bound in the DuxOE condition further demonstrating the specificity of this method (Figure 4b;
244 right). To rank the biological relevance of the individually changed binding sites between
245 control and DuxOE conditions, we linked all annotated gene loci to RNA expression. A striking

246 correlation between the gain-of-footprint and gain-of-expression of corresponding loci was
247 clearly observed and mirrored by the TOBIAS predicted bound/unbound state (Figure 4c).
248 Amongst the genes within the list of bound Dux binding sites (Supp. Table 5 for full Dux target
249 list) were well known Dux targets including *Zscan4c* and *Pramef25* [45], for which local
250 footprints for Dux were clearly visible (Figure 4d). The high resolution of footprints is
251 particularly pronounced for *Tdpoz1* which harbors two potential Dux binding sites of which one
252 is clearly footprinted in the score track, while the other is predicted to be unoccupied (Figure
253 4d; bottom). In line with this, *Tdpoz1* expression is significantly upregulated upon DuxOE as
254 revealed by RNA-seq (log2FC: 6,95). Consistently, *Tdpoz1* expression levels are highest at
255 2C in zygotes and decrease thereafter, strongly indicating that *Tdpoz1* is likely a direct target
256 of Dux during PD both *in vitro* and *in vivo* [31, 46] (Supp. Table 5). Footprinting scores also
257 directly correlated with ChIP-seq peaks for Dux in the *Tdpoz1* promoter (Supp. Figure 4a), an
258 observation which we also found at many other positions (Examples shown in Supp. Figure
259 4b+c).

260 Many of the TOBIAS-predicted Dux targets encode TFs themselves. Therefore, we applied
261 the TOBIAS network module to subset and match all activated binding sites to TF target genes
262 with the aim of inferring how these TF activities might connect. Thereby, we could model an
263 intriguing pseudo timed TF activation network. This directed network uncovered a TF
264 activation cascade initiated by Dux, resulting in the activation of 7 primary TFs which appear
265 to subsequently activate 32 further TFs (first three layers depicted in Figure 4e). As Dux is a
266 regulator of ZGA, we asked how the *in vitro* activated Dux network compared to gene
267 expression throughout PD *in vivo*. Strikingly, the *in vivo* RNA-seq data of the resolved
268 developmental dataset [31] confirmed an early 2C specific expression for Dux, followed by a
269 slightly shifted activation pattern for all direct Dux targets except for *Rxrg* (Figure 4f). However,
270 it is of note that *Rxrg* is significantly upregulated in the *in vitro* DuxOE from which the network
271 is inferred (Supp. Table 5), pointing to both the similarities and differences between the *in vivo*
272 2C and *in vitro* 2C-like stages induced by Dux. In conclusion, these data show that beyond

273 identifying specific target genes of individual TFs, TOBIAS can infer biological insight by
274 predicting entire TF activation networks.

275 Notably, many of the predicted Dux binding sites (40%) are not annotated to genes (Figure
276 4g), raising the question what role these sites play in ZGA. Dux is known to induce expression
277 of repeat regions such as LTRs [5] and consistently, we found that more than half of the DUX-
278 bound sites are indeed located within known LTR sequences (Figure 4g) which were
279 transcribed both *in vitro* and *in vivo* (Figure 4h). Interestingly, we found that 28% of all Dux
280 binding sites overlap with genomic loci encoding LINE1 elements. Although LINE1 expression
281 does not appear to be altered in mESC cells, there is a striking pattern of increasing LINE1
282 transcription from 4C-8C (Figure 4h) *in vivo*, pointing to a possible role of LINE1 regulation
283 throughout PD. Finally, we found that 6% of the Dux binding sites do not overlap with any
284 annotated gene nor with putative regulatory repeat sequences, even though transcription
285 clearly occurs at these sites (Figure 4h bottom). One example is a predicted Dux binding site
286 on chromosome 13, which coincides with a spliced region of increased expression between
287 control mESC/DuxOE and comparable high expression in 2C, 4C and 8C (Supp. Figure 5).
288 These data clearly indicate the existence of novel transcribed genetic elements, the function
289 of which remains unknown, but which are likely controlled by Dux and could play a role during
290 PD.

291 In conclusion, TOBIAS predicted the exact locations of Dux binding in promoters of target
292 genes, and could unveil how Dux initiates TF-activation networks and induces expression of
293 repeat regions. Importantly, these data further show that TOBIAS can identify any TFBS with
294 increased binding, not only those limited to annotated genes, which aids in uncovering novel
295 regulatory genetic elements.

296

297 **Discussion**

298 **Footprint scores reveal true characteristics of protein binding**

299 To the best of our knowledge, this is the first application of a DGF approach to visualize gain
300 and loss of individual TF footprints in the context of time series, TF overexpression, and TF-
301 DNA binding for a wide-range of TFs in parallel. Importantly, we found that these advances
302 could in large part be attributed to the framework approach we took in developing TOBIAS,
303 which enabled us to simultaneously compare global TF binding across samples and quantify
304 changes in TF binding at specific loci. The modularity of the framework also allowed us to
305 apply a multitude of downstream analysis tools to easily visualize footprints and gain even
306 more information about TF binding dynamics as exemplified by the discovery of the Dux TF-
307 activation network.

308 The power of this framework to handle time-series data becomes especially apparent when
309 correlating the TOBIAS-based prediction of TF binding to RNA-seq data from the same time
310 points. For instance, TOBIAS could infer when the maternally transferred TF SALL4 is truly
311 active while its gene expression pattern alone does not allow to make such conclusions. Along
312 this line, TOBIAS is also powerful in circumstances where gene expression of a particular TF
313 appears to be anticorrelated with its binding activity. It is tempting to speculate that TFs for
314 which footprinting scores are low, even though their RNA expression is high, might act as
315 transcriptional repressors, because footprinting relies on the premise that TFs will increase
316 chromatin accessibility around the binding site. In support of this hypothesis, recent
317 investigations have suggested that repressors display a decreased footprinting effect in
318 comparison to activators [23]. Therefore, the integration of ATAC-seq footprinting and RNA-
319 seq is an important step in revealing additional information such as classification TFs into
320 repressors and activators, as well as the kinetics between expression and binding.

321

322 **Species-specific TFs use common ZGA motifs in mice and human**

323 By integration of human and murine TF activities using both differential footprinting and
324 species-specific TFBS overlaps, our analyses revealed that the majority of TF motifs are active

325 at corresponding timepoints of human and mouse ZGA. This is not necessarily surprising since
326 homologous TFs that exert the same functions usually use similar motifs (e.g Pou2f1/POU2F1,
327 Otx1/OTX1 and/or Foxa3/FOXA3). Interestingly though, we found that this is not the case for
328 all TF motifs. In this context, we found that the human RHOXF1 motif (Figure 2b) is likely not
329 utilized by Rhox proteins in mice even though more than 30 Rhox genes exists. Evidently,
330 throughout multiple duplications, Rhox genes seem to have obtained other functionalities in
331 mouse [47] in comparison to the two human RHOX genes that are expressed in reproductive
332 tissues [48]. Therefore, although we found the human RHOXF1 motif to be highly active in
333 mice, this motif is most likely utilized by other proteins such as the mouse specific Obox
334 proteins. In support of this conclusion, expression patterns of Obox proteins appear to be
335 tightly regulated during PD [49] ([31]). High expression of Obox 1/2/5/7 is observed from the
336 zygote to 4C stage, while Obox3/6/8 are expressed and peak at later stages (Supp. Table 4).
337 Notably, there is a significant sequence similarity of the homeobox domains but not in the
338 other parts of the RHOXF1 and Obox protein sequences, which supports the similarity in
339 binding specificity. Although the potential functional overlap of RHOXF1 and Obox factors
340 remains unresolved, our inter-species analysis suggests an unappreciated function of these
341 factors and their targets during PD, clearly warranting an in depth investigation.

342 In the context of TF target prediction, the power of TOBIAS was particularly highlighted by the
343 fact that the analysis could identify almost all known Dux targets. In addition to coding genes,
344 our analysis disclosed novel Dux binding sites and significant footprint scores at LINE1
345 encoding genomic loci, which appear to be activated at the 4C/8C stage. This finding is
346 especially interesting because a recent study has shown that LINE1 RNA can interact with
347 Nucleolin and Kap1 to repress Dux expression [50]. Therefore, our findings give rise to a
348 kinetics driven model in which Dux not only initiates ZGA but also regulates its own termination
349 by a temporally delayed negative feedback loop. How this feedback loop is exactly controlled
350 remains to be determined.

351 **Limitations and outlook of footprinting analysis**

352 Despite the striking capability of DGF analysis, some limitations and dependencies of this
353 method still remain. Amongst these is the need of high-quality TF motifs for matching footprint
354 scores to individual TFs with high confidence. In other words, while the binding of a TF might
355 create an effect that can be interpreted as a footprint, without a known motif, this effect cannot
356 be matched to the corresponding TF. This becomes evident in the context of DPPA2/4, a TF
357 described by several groups to act in PD and even upstream of Dux [44]. DPPA2/4 targets
358 GC rich sequences [44], but its canonical binding motif remains unknown. It also needs to be
359 noted that footprinting analysis cannot take effects into account that arise from heterogeneous
360 mixtures of cells wherein TFs are bound in some cells and in others not. Therefore, if not
361 separated, the classification of differential binding will be an observation averaged across
362 many cells, possibly masking subpopulation effects. Recent advances have enabled to
363 perform ATAC-seq in single cells [51], but this generates sparse matrices, rendering
364 footprinting approaches on single cells illusive. However, we speculate that by creating
365 aggregated pseudo-bulk signals from large clustered SC ATAC datasets, DGF analysis might
366 also become possible in single cells.

367

368 **Conclusions**

369 Here, we have illustrated the TOBIAS framework as a versatile tool for ATAC-seq analysis
370 which helps to unravel transcription factor binding dynamics in complex experimental settings
371 that are otherwise difficult to investigate. We showed that entire networks of TF binding, which
372 have previously been explored using a combination of omics methods, can be recapitulated
373 to a great extent by DGF analysis, which requires only ATAC-seq and TF motifs. From a global
374 perspective, we provided new insights into PD by quantifying the stage-specific activity of
375 specific TFs. Furthermore, we highlighted the usage of TOBIAS to study specific transcription
376 factors as exemplified by our investigations on Dux. Finally, we used the specific TF target

377 predictions to gain insights into the local binding dynamics of Dux in the context of TF-
378 activation networks, repeat regions and novel genetic elements.

379 In conclusion, we present TOBIAS as the first comprehensive software that performs all steps
380 of DGF analysis, natively supports multiple experimental conditions and performs visualization
381 within one single framework. Although we utilized the process of PD as a proof of principle,
382 the modularity and universal nature of the TOBIAS framework enables investigations of
383 various biological conditions beyond PD. We believe that continued work in the field of DGF,
384 including advances in both software and wet-lab methods, will validate this method as a
385 versatile tool to extend our understanding of a variety of epigenetic processes involving TF
386 binding.

387
388
389
390
391
392

393 **Declarations**

394 **Ethics approval and consent to participate**

395 Not applicable.

396 **Consent for publication**

397 Not applicable.

398 **Availability of data and materials**

399 The TOBIAS software is available on GitHub at: <https://github.com/loosolab/TOBIAS>.

400 Excerpts of the data analyzed here are accessible for dynamic visualization at:

401 <http://loosolab.mpi-bn.mpg.de/tobias-meets-wilson>. All raw data analyzed are available from

402 GEO or ENCODE as described in Methods. The complete TOBIAS output for the analysis of

403 the Dux overexpression dataset can be downloaded from:

404 [https://figshare.com/projects/Digital_Genomic_Footprinting_Analysis_of_ATAC-](https://figshare.com/projects/Digital_Genomic_Footprinting_Analysis_of_ATAC-seq_dataset_from_preimplantation_timepoints_via_TOBIAS/69959)
405 [seq_dataset_from_preimplantation_timepoints_via_TOBIAS/69959](https://figshare.com/projects/Digital_Genomic_Footprinting_Analysis_of_ATAC-seq_dataset_from_preimplantation_timepoints_via_TOBIAS/69959).

406 **Competing interests**

407 None to declare

408 **Funding**

409 This work was funded by the Max Planck Society, the German Research Foundation (DFG),
410 grant KFO309 (project number 284237345, epigenetics core unit) to ML, and by the Cardio-
411 Pulmonary Institute (CPI), EXC 2026, Project ID: 390649896 to ML.

412 **Authors' contributions**

413 MB, CK, JK and ML wrote the manuscript. MB, PG, HS, AP, KK, AF and JP performed the
414 bioinformatics analysis. JK, TB and ML directed, coordinated and supervised the work.

415 **Acknowledgements**

416 We would like to thank the IT-group at MPI-BN for continued support with IT-infrastructure.
417 We would also like to thank Marius Dieckmann, the administrator of the Kubernetes cluster
418 in Gießen, for his support and help in implementing the TOBIAS-Nextflow Cloud version.

419 **Methods**

420

421 **Datasets**

Organism	Deposited data	Source	Identifier
Mouse	ATAC-seq, RNA-seq and ChIP-seq from mESC control and Dux overexpression	[5]	GEO: GSE85632
Mouse	ATAC-seq and RNA-seq from various preimplantation stages	[31]	GEO: GSE66390

Human	ATAC-seq and RNA-seq from various preimplantation stages	[30]	GEO: GSE101571
-------	--	------	-------------------

422

423 For all public data sets used in this study (see table above), raw files were obtained from the
424 European Nucleotide Archive [52] and processed as described in the methods section. See
425 also methods section “Comparison of TOBIAS to existing methods” for links to the ENCODE
426 data used for method validation.

427

428 Processing of ATAC-seq data

429 Raw sequencing fastq files were assessed for quality, adapter content and duplication rates
430 with FastQC v0.11.7, trimmed using cutadapt [53] and aligned with STAR v2.6.0c [54]
431 (parameters: “--alignEndsType EndToEnd --outFilterMismatchNoverLmax 0.1 --
432 outFilterScoreMinOverLread 0.66 --outFilterMatchNminOverLread 0.66 --outFilterMatchNmin
433 20 --alignIntronMax 1 --alignSJDBoverhangMin 999 --alignEndsProtrude 10 ConcordantPair -
434 -alignMatesGapMax 2000 --outMultimapperOrder Random --outFilterMultimapNmax 999 --
435 outSAMmultNmax 1”) to either the mouse or human genome using Mus_musculus.GRCm38
436 or Homo_sapiens.GRCh38 versions from Ensembl [55]. Accessible regions were identified by
437 peak calling for each sample separately using MACS2 (parameters: “--nomodel --shift -100 --
438 extsize 200 --broad”) [56]. Peaks from each sample were merged to a set of union peaks
439 across all conditions using “bedtools merge”. Each union peak was annotated to the
440 transcriptional start site of genes (GENCODE [57]) in a distance of -10000/+1000 from the
441 TSS using UROPA [58].

442 Processing of RNA-seq data

443 Raw reads were assessed for quality, adapter content and duplication rates with FastQC
444 v0.11.7, trimmed using cutadapt [53] and aligned with STAR v2.6.0c [54] (parameters: “--
445 outFilterMismatchNoverLmax 0.1 --outFilterScoreMinOverLread 0.9 --

446 outFilterMatchNminOverLread 0.9 --outFilterMatchNmin 20 --alignIntronMax 200000 --
447 alignMatesGapMax 2000 --alignEndsProtrude 10 ConcordantPair --outMultimapperOrder
448 Random --outFilterMultimapNmax 999”) to either the mouse or human genome using
449 Mus_musculus.GRCm38 or Homo_sapiens.GRCh38 versions from Ensembl [55].
450 Differentially expressed genes were identified using DESeq2 v1.22 [59]. Only genes with a
451 minimum log₂ fold change of ± 1 , a maximum Benjamini–Hochberg corrected P-value of 0.05
452 and a minimum combined mean of five reads were classified as significantly differentially
453 expressed.

454 Processing of ChIP-seq data

455 Raw sequencing files in fastq format were quality assessed by Trimmomatic by trimming reads
456 after a quality drop below a mean of Q15 in a window of 5 nucleotides [60]. All reads longer
457 than 15 nucleotides were aligned versus the mouse genome version mm10, keeping just
458 unique alignments (parameters: --outFilterMismatchNoverLmax 0.2 --
459 outFilterScoreMinOverLread 0.66 --outFilterMatchNminOverLread 0.66 --outFilterMatchNmin
460 20 --alignIntronMax 1 --alignSJDBoverhangMin 999 --outFilterMultimapNmax 1 --
461 alignEndsProtrude 10 ConcordantPair) by using the STAR mapper [54]. Read deduplication
462 was done by Picard (<http://broadinstitute.github.io/picard/>).

463 Processing of transcription factor motifs

464 TF motifs were downloaded from JASPAR CORE 2018 [61], the JASPAR PBM HOMEO
465 collection and Hocomoco V11 [62] databases. We further included the human ARGFX_3 motif
466 from footprintDB [63] which originates from a HT-SELEX assay [64]. In addition to the
467 Dux/Dux4 motifs of JASPAR and Hocomoco, we also included two TF motifs for MDUX/DUX4
468 created using MEME-ChIP [65] with standard parameters on the ChIP-seq peaks of [45]
469 (GSE87279).

470 JASPAR motifs were linked to Ensembl gene ids by mapping the provided “Uniprot id” to the
471 “Ensembl gene id” through biomaRt [66]. Hocomoco motifs were likewise linked to genes
472 through the provided HGNC/MGI annotation. Due to the redundancy of motifs between
473 JASPAR and Hocomoco, we further filtered the TF motifs to one motif per gene, preferentially
474 choosing motifs originating from mouse/human respectively. For each TOBIAS run, we
475 created sets of expressed TFs as estimated from RNA-seq in the respective conditions. This
476 amounted to 590 motifs for the dataset on human preimplantation stages, 464 motifs for the
477 dataset on mouse preimplantation, and 459 for the DuxOE dataset.

478 Maternal genes

479 Maternal genes for human and mouse were downloaded from the REGULATOR database
480 [32]. Entrez gene ids were converted to Ensembl gene ids using biomaRt [66] and
481 subsequently matched to available TF motifs.

482 Overlap of Dux binding sites to repeat elements

483 Repeat elements for mm10 were downloaded from UCSC
484 (<http://hgdownload.soe.ucsc.edu/goldenPath/mm10/database/rmsk.gz>). Overlap of Dux sites
485 to individual repeat elements (as seen in figure 4G) was performed using “Bedtools intersect”.
486 The sum of overlaps were counted by repeat class (LINE1/LTR).

487 Visualization

488 All TF-score heatmaps were generated by R Version 3.5.3 and complex heatmap package
489 version 3.6 [67]. Individual gene views were generated by loading TOBIAS output tracks into
490 IGV version 2.6.2 [68] or using the svist4get visualization tool [69]. TF networks were drawn
491 with Cytoscape version 3.7.1 [70]. Heatmaps of genomic signal density were generated using
492 Deeptools version 3.3.0 [71]. All other figures, such as footprint plots, volcano plots and motif
493 clustering dendrograms were generated by the TOBIAS visualization modules as described
494 below.

495 The TOBIAS framework

496 In developing TOBIAS, we found that there were six main areas of DGF which had not been
497 comprehensively addressed in the context of ATAC-seq footprinting analysis:

- 498 ● All-in-one framework including bias correction, footprinting, quantification of protein
499 binding and visualization
- 500 ● Investigation of TF binding on a global level (which TFs are more bound globally) as
501 well as the locus-specific level (which TF binds to which genomic locations including
502 statistics on differential binding)
- 503 ● Consideration of the redundancy and similarity of known TF binding motifs in the
504 context of footprinting
- 505 ● A scoring model for TF-DNA binding taking into account the potential lack of a
506 canonical footprint effect
- 507 ● Comparison and quantification of TF binding activity within complex experimental
508 settings (multiple conditions or time series)
- 509 ● All in one automated workflows for recurring analysis tasks

510

511 Modules enabling these individual analysis steps are included in the TOBIAS package, which
512 is publicly available at Github (<https://github.com/loosolab/TOBIAS>) as well as on PyPI and
513 Bioconda. Besides the examples given in the repository README, we also provide a Wiki
514 (<https://github.com/loosolab/TOBIAS/wiki>) which introduces some of the individual software
515 modules. We used the pre-defined workflows in Snakemake and NextFlow to run the full
516 analysis. The single modules are explained in more detail below.

517 **Bias correction (TOBIAS ATACCorrect module)**

518 Each Tn5-cut site is defined as the 5' end of the read shifted by +5 at the plus strand and -4
519 at the minus strand to center the transposase event. Using the mapped reads from closed
520 chromatin, ATACCorrect builds a dinucleotide weight matrix [72] representing the preference of
521 Tn5 insertion. In contrast to the classical position weight matrix (PWM) the dinucleotide weight

522 matrix (DWM) captures the inter-base relationships which arise due to the palindromic nature
 523 of the bias. A background model is similarly built by shifting all reads +100bp as described by
 524 [17].

525 Reads within open chromatin peaks are then corrected by estimating the expected number of
 526 cuts per base pair and subtracting this from the observed cut sites as follows (modified from
 527 [24]):

$$528 \quad c_i = x_i - e_i$$

529 where

$$530 \quad e_i = \hat{x}_i * \hat{b}_i, \quad \hat{x}_i = \sum_{j=i-50}^{i+50} x_j, \quad \hat{b}_i = \frac{b_j}{\sum_{j=i-50}^{i+50} b_j}$$

531 where x_i is the observed cut sites, e_i is the expected cut sites, b_i is the calculated bias level,
 532 and c_i is the corrected cut sites at position i . To limit the influence of low-bias positions in the
 533 calculation of \hat{b}_i , a lower limit is set for b_i by calculating the fit of cutsites vs. bias to a rectified
 534 linear unit function (ReLU) in moving 100bp-windows and setting every b_i below the linear fit
 535 to 0. This calculation is performed for all base pairs within open chromatin, setting all other
 536 positions to 0. Lastly, each c_i is rescaled to fit the original sum of cuts \hat{x}_i for each window.

537 Footprinting (TOBIAS ScoreBigwig module)

538 We estimate footprint scores across open chromatin regions by calculating:

$$539 \quad FP = \bar{x}_{flank} - \bar{x}_{mid}$$

540 where

$$541 \quad \bar{x}_{flank} = \frac{\sum_{i=j}^{j+wf} x_i + \sum_{i=j+wf+wm}^{j+2*wf+Wm} x_i}{2 * wf} \text{ for } x_i > 0,$$

$$542 \quad \bar{x}_{mid} = \frac{\sum_{i=j+wf}^{j+wf+wm} x_i}{wm} \text{ for } x_i < 0$$

543 x_i is the number of cuts at position i , wf = width of flank in bp, wm = width of middle (footprint)
544 in bp. The defaults used are: $wf = [10;30]$, $wm = [20;50]$.

545 The term \bar{x}_{mid} will be negative and will therefore raise the score if there is a high depletion of
546 cuts in the footprint (middle). If there is no depletion, the score will simplify to the mean of cuts
547 in the flanking regions, representing accessibility. It is therefore not necessary to see a
548 canonical footprint shape for the footprint score to be high. The footprint score can be
549 interpreted as higher scores being more evidence that a protein was bound at a given position.
550 All calculations are done by the TOBIAS “ScoreBigwig” module.

551 **Estimation of transcription factor states and pairwise comparison between conditions** 552 **(TOBIAS BINDetect module)**

553 To match the calculated footprint scores to potential binding sites, TOBIAS BINDetect
554 integrates genomic sequence, footprint scores from several conditions and motifs to identify
555 up- and down regulated TFs based on footprint scores.

556 In the first step of the algorithm, the MOODS library (<https://github.com/jhkorhonen/MOODS>
557 [73]) is used to detect TF binding sites (within peaks) with a p-value threshold of $1e-4$.
558 Background base pair probabilities are estimated from the input peak set. Subsequently, each
559 binding site is matched to footprint scores for each condition. Simultaneously, a background
560 distribution of values is built by randomly subsetting peak regions at ~ 200 bp intervals, and the
561 scores from each condition are normalized to each other using quantile normalization. These
562 values are used to calculate a distribution of background log2FCs for each pairwise
563 comparison of conditions.

564 Overlaps between the TFBS identified in the first step are quantified by creating a distance
565 matrix of TFs. The distance between a TF pair (TF1;TF2) is calculated as:

566

$$567 \text{dist}_{TF1;TF2} = 1 - \max(\text{overlap}_{TF1;TF2} / \text{total}_{TF1}, \text{overlap}_{TF2;TF1} / \text{total}_{TF2})$$

568

569 where $total_{TF1}$ and $total_{TF2}$ are the total basepairs of all $TF1$ and $TF2$ sites respectively
570 and $overlap_{TF1;TF2}$ is the amount of base pairs of $TF1$ which overlap with $TF2$ sites. The
571 max-statement ensures that the overlap is calculated with regards to the shortest TF motif.

572 In the second step of the algorithm, every TF binding site found (for each motif given as input)
573 is split into bound and unbound sites based on a score threshold per condition. The threshold
574 is set at the level of significance of a normal-distribution fit to the background distribution of
575 scores (user-defined p-value). As well as the per-condition split, each site is assigned a
576 log2FC (fold change) per comparison, which represents whether the binding site has
577 larger/smaller footprint scores in comparison. The global distribution of log2FC's per TF is
578 compared to the background distributions to calculate a *differential binding score*, which is
579 calculated as:

$$\frac{(\bar{x}_o - \bar{x}_b)}{((std_o + std_b) / 2)}$$

580

581 where \bar{x}_o, std_o and \bar{x}_b, std_b are the means and standard deviations of the observed and
582 background log2FC distributions respectively. A p-value is also calculated by subsampling
583 100 log2FCs from the background and calculating the significance of the observed change
584 (Python's `scipy.stats.ttest_1samp`). By comparing the observed log2FC distribution to the
585 background log2FC, the effects of any global differences due to sequencing depth, noise etc.
586 are controlled.

587 The differential binding scores and p-values are visualized as a volcano plot per condition-
588 comparison. All TFs with $-\log_{10}(\text{pvalue})$ above the 95% quantile or differential binding scores
589 smaller/larger than the 5% and 95% quantiles (top 5% in each direction) are colored and
590 shown with labels. Below the plot, hierarchical clustering of the TFBS-distance matrix is shown
591 and all TFs with distances less than 0.5 (overlap of 50% of bp) are colored as separate
592 clusters.

593 The result of BINDetect is a folder-structure containing an overview of all potential binding
594 sites (as .bed as well as excel files), the predicted split into bound and unbound sites, and a
595 global overview of differentially bound TFs per condition-comparison.

596 **Visualizing aggregate plots and calculation of footprint depth (TOBIAS PlotAggregate** 597 **module)**

598 Footprints are visualized using the subtool “TOBIAS PlotAggregate”. Aggregate footprints are
599 created by aligning genomic signals centered on all binding sites (taking into account
600 strandedness), to create a matrix of (n sites) x (n bp). The aggregate signal is calculated as
601 the mean of each column (each bp). The default of +/- 60bp from the motif center was used
602 throughout this manuscript.

603 The aggregate footprinting depth (FPD), which is applied in Supp. Figure 2c-d, was calculated
604 for each TF as:

$$605 \quad FPD = \overline{signal_{flank}} - \overline{signal_{middle}}$$

606
607 where $\overline{signal_{middle}}$ is the mean of the signal centered on the TFBS (30bp) and $\overline{signal_{flank}}$
608 is the mean of the signal in the remaining flanks ([-60;-15] and [+15;+60] bp) (See Supp. Figure
609 2b).

610

611 Similarly to the investigations in previous literature [22], we applied a mixture model from the
612 Mixtools R package [74] to estimate the fractions of TFs with/without measurable footprints
613 (Supp. Figure 2e).

614 **Transcription factor binding network (TOBIAS CreateNetwork module)**

615 The TF-TF network for Dux was built by subsetting all binding sites on the following
616 characteristics: Bound in the promoter of a target gene, labeled “Unbound” in Control, labeled
617 “Bound” in DuxOE, and log2FC footprint score increasing for DuxOE vs. Control. All targets
618 were further reduced to only include genes encoding TFs with available motifs. Motifs were
619 matched to genes as explained in the methods section “Processing of transcription factor
620 motifs”. The network was then created using “TOBIAS CreateNetwork”. The result is a network
621 of source and target nodes with directed edges, which in words can be described as: (Source
622 TF) binds in the promoter of (Target TF).

623 **TOBIAS framework output structure**

624 The output generated by the TOBIAS framework is organized in a hierarchical folder structure,
625 which increases clarity of all steps of the analysis. The folder structure specifically organizes
626 input data, pre-processing output like peak-calling and annotation, genomic tracks such as
627 bias correction and footprints, as well as the local and global TF predictions. Particularly, the
628 output for every individual TF investigated is arranged into separate folders containing TF
629 specific plots, annotations and binding predictions. This structure makes it simple to use the
630 output for further downstream analysis, as was showcased in this work. An exemplary output
631 of the complete framework can be found at:
632 [https://figshare.com/projects/Digital_Genomic_Footprinting_Analysis_of_ATAC-](https://figshare.com/projects/Digital_Genomic_Footprinting_Analysis_of_ATAC-seq_dataset_from_preimplantation_timepoints_via_TOBIAS/69959)
633 [seq_dataset_from_preimplantation_timepoints_via_TOBIAS/69959](https://figshare.com/projects/Digital_Genomic_Footprinting_Analysis_of_ATAC-seq_dataset_from_preimplantation_timepoints_via_TOBIAS/69959)

634 Validation

635 **Comparison of TOBIAS to existing methods**

636 Although footprinting tools for DNase-seq exist [18, 75, 76] [24, 77-79] [80], we have focused
637 our comparison on tools which are easily obtainable and installable, do not require ChIP-seq
638 training-data, and are explicitly supporting ATAC-seq. We have additionally added two metrics
639 for “peak strength” and “PWM score” to compare TOBIAS to other footprinting-free metrics.
640 The validation datasets and usage of existing tools are described in the following sections.

641 **Datasets**

642 The TOBIAS framework was benchmarked using ATAC-seq data for the GM12878 cell line
643 (GEO: GSE47753) and TF ChIP-seq data from ENCODE for the same cell line. ATAC-seq
644 data was prepared as explained in the section “Processing of ATAC-seq data”. ChIP-seq peak
645 peak regions were downloaded and associated to motifs from Jaspar CORE 2018 using
646 “MEME Centrimo” [81]. Only ChIP-seq experiments with motif enrichment $> 1.0e-100$
647 (Centrimo E-value) were kept. The pairing of the remaining 36 motifs and ChIP-seq peaks is
648 seen below:

ENCODE accession	TF name	JASPAR motif ID
ENCSR987MTA	BHLHE40	MA0464.2
ENCSR681NOM	CEBPB	MA0466.2
ENCSR839XZU	Crem	MA0609.1
ENCSR000DZN	CTCF	MA0139.1
ENCSR000DZQ	EBF1	MA0154.3
ENCSR841NDX	ELF1	MA0473.2
ENCSR000DZB	ELK1	MA0028.2
ENCSR000BKA	ETS1	MA0098.3
ENCSR626VUC	ETV6	MA0645.1
ENCSR331HPA	Gabpa	MA0062.2

ENCSR009MBP	HSF1	MA0486.2
ENCSR000DYS	JUND	MA0491.1
ENCSR000DYV	MAFK	MA0496.2
ENCSR000DZF	MAX	MA0058.3
ENCSR000BKB	MEF2A	MA0052.3
ENCSR000BNG	MEF2C	MA0497.1
ENCSR000DZI	MXI1	MA1108.1
ENCSR000DNM	NFYB	MA0502.1
ENCSR514VYD	NR2F1	MA0017.2
ENCSR000DZO	NRF1	MA0506.1
ENCSR000BHD	PAX5	MA0014.3
ENCSR000BGR	PBX3	MA1114.1
ENCSR711XNY	PKNOX1	MA0782.1
ENCSR000BGF	REST	MA0138.2
ENCSR000BRI	RUNX3	MA0684.1
ENCSR041XML	SRF	MA0083.3
ENCSR739IHN	TBX21	MA0690.1
ENCSR000BGZ	Tcf12	MA0521.1
ENCSR501DKS	Tcf7	MA0769.1
ENCSR000BGI	USF1	MA0093.2
ENCSR000DZU	USF2	MA0526.2
ENCSR000BNP	YY1	MA0095.2
ENCSR000BHC	ZBTB33	MA0527.1
ENCSR000DZL	ZNF143	MA0088.2
ENCSR072PWP	ZNF24	MA1124.1
ENCSR000DYP	ZNF384	MA1125.1

649

650 Bound binding sites per TF were defined as any TFBS within +/- 100bp from the paired ChIP-

651 seq peak summit. In case of two or more binding sites per peak, the one closest to the summit

652 was set to bound, and others were excluded. Unbound binding sites were defined as any
653 TFBS not overlapping any ChIP-seq peak, as well as not overlapping bound sites from any
654 other factors.

655 **Bias correction approaches**

656 TOBIAS was compared to the existing bias correction methods as follows:

657 • **seqOutBias** ([25])

658 The seqOutBias software was downloaded from GitHub
659 (<https://github.com/guertinlab/seqOutBias>). Following the vignette for ATAC-seq,
660 mappability files were created and ATAC-seq reads were corrected for plus/minus
661 strand reads separately. After correction, we further shifted the positive and negative
662 tracks +5 and -4bp respectively, as this was not performed by the tool itself.

663 • **HINT-ATAC** ([16])

664 The HINT software was downloaded from PyPI as part of the RGT software suite. Bias-
665 correction was performed from the ATAC-seq reads using the command “rgt-hint
666 tracks --bc --bigWig <bam>”.

667

668 Aggregate footprints for each method across all (within peaks), bound and unbound binding
669 sites (see explanation above) were visualized using “TOBIAS PlotAggregate”.

670

671 **Footprinting**

672 For comparing TOBIAS to existing footprinting methods as follows:

673 • **msCentipede** ([14])

674 The msCentipede software was downloaded from GitHub
675 (<https://github.com/rajanil/msCentipede>). For each TF, the binding model was built
676 using the 5000 TFBS with highest PWM score genomewide. The resulting models
677 were then used to infer the posterior binding-probability of TFBS in peaks.

678 • **Wellington ([76])**

679 The pyDNase software was downloaded from PyPI. Footprints in ATAC-seq peaks
680 were estimated using “wellington_footprints.py” with the “-A” option for ATAC-seq
681 mode.

682 • **Peak** **strength**

683 The “Peak strength” metric is defined as the mean number of Tn5 insertions in the
684 ATAC-seq peak where the binding site is found. This score represents the accessibility
685 of a certain region not taking into account local footprint information.

686 • **PWM** **score**

687 The score of the motif-sequence match at the specific TFBS. As this is based on
688 sequence alone, the PWM-score is independent of chromatin accessibility.

689

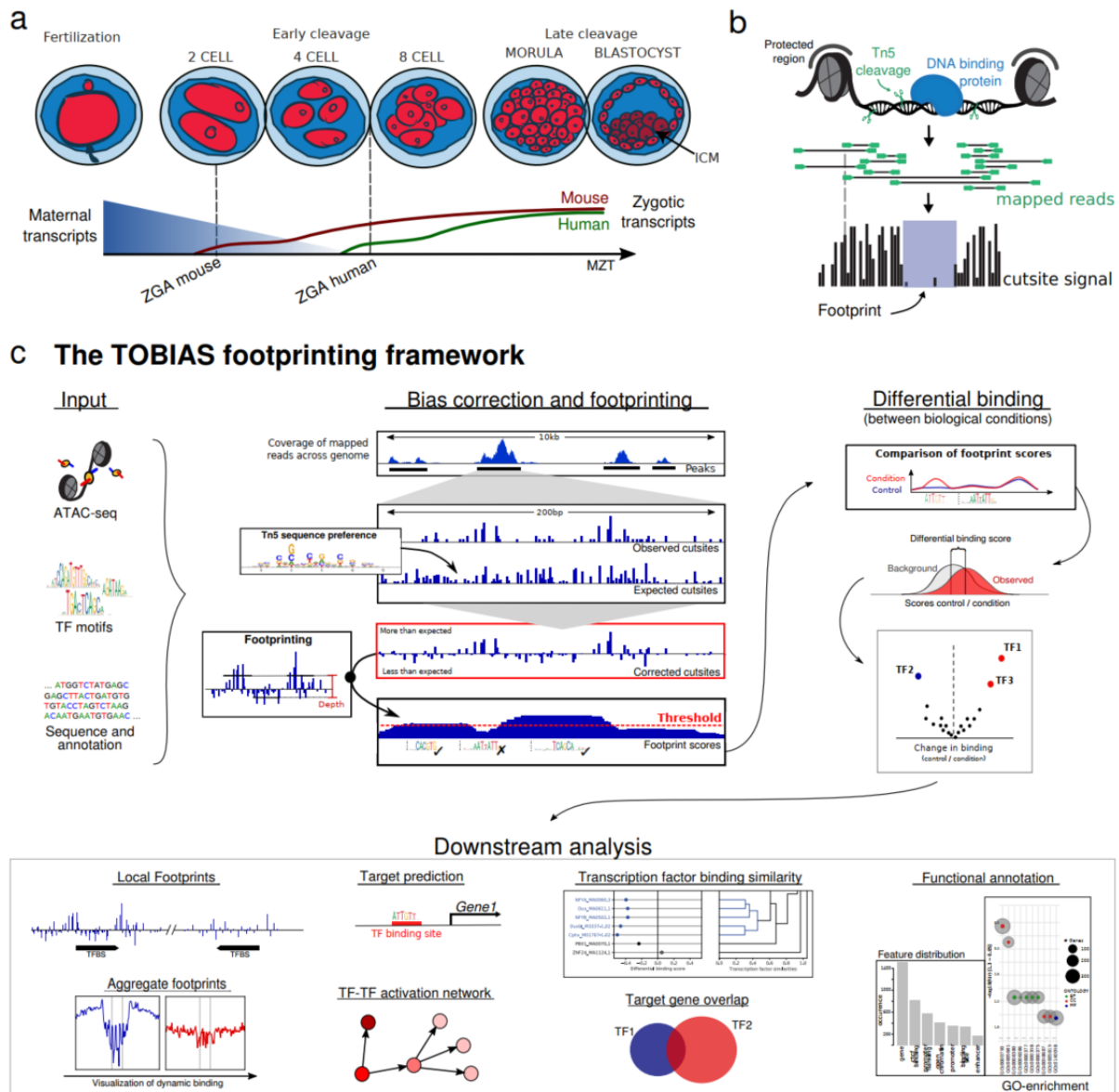
690 The area under the ROC curve (auROC) was used to evaluate the predictive power of each
691 method.

692 **Note on comparison:** Overall, we find that TOBIAS performs at least equally well in
693 comparison to msCentipede [14], a learning based approach, that demands high
694 computational performance and individually trained models for every TF under investigation
695 (Supp. Figure 1b). Of note, although this learning-based approach performs well overall, it
696 exhibits a drastic loss of predictive power for some TFs, while the TOBIAS scoring model
697 provides robust binding prediction scores even for those TFs that do not leave visible footprints
698 at first glance (Supp. Figure 1b right).

699

700

701 Figures and figure legends



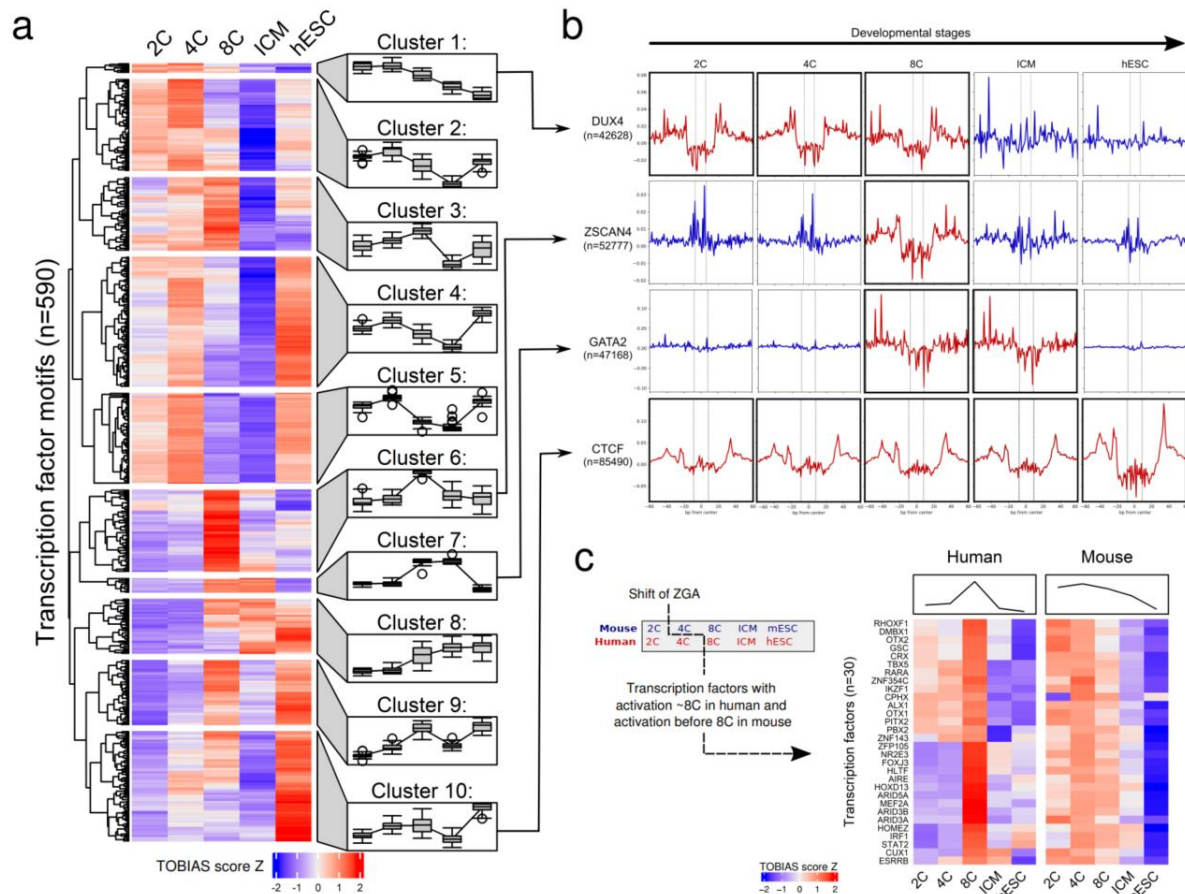
702

703 **Figure 1: The use of chromatin accessibility assays to investigate early developmental**
 704 **processes**

705 **(a) Early embryonic development in human and mouse.** The fertilized egg undergoes a series of
 706 divisions ultimately creating the structure of the blastocyst. While maternal transcripts are depleted, the
 707 zygotic genome is activated in waves as indicated by the dark shading. ZGA initiates in mouse at 2-cell
 708 stage and in human at the 4-8-cell stage.

709 **(b) The concept of footprinting using ATAC-seq.** The Tn5 transposase cleaves and inserts
 710 sequencing adapters in open chromatin, but is unable to cut in chromatin occupied by e.g. nucleosomes

711 *or transcription factors. The mapped sequencing reads can be used to create a signal of single Tn5-*
712 *events (cutsites), in which binding of transcription factors is visible as depletion of signal (the footprint).*
713 **(c) The TOBIAS digital genomic footprinting framework.** *Using an input of sequencing reads from*
714 *ATAC-seq, transcription factor motifs and sequence information, the TOBIAS footprinting framework*
715 *detects local and global changes in transcription factor binding. Bias-correction of the Tn5 sequence*
716 *preference enables detection of local chromatin footprints and matching to individual TFBS. Footprint*
717 *scores can be compared between conditions and are used to define differential binding in pairwise*
718 *comparisons. The global binding map allows for a variety of downstream analysis such as*
719 *visualization of local and aggregated footprints across conditions, prediction of target genes for each*
720 *TF as well as comparison of binding specificity between several transcription factors. Functional*
721 *annotation such as GO enrichment can be used to infer biological meaning of target gene sets.*
722



723

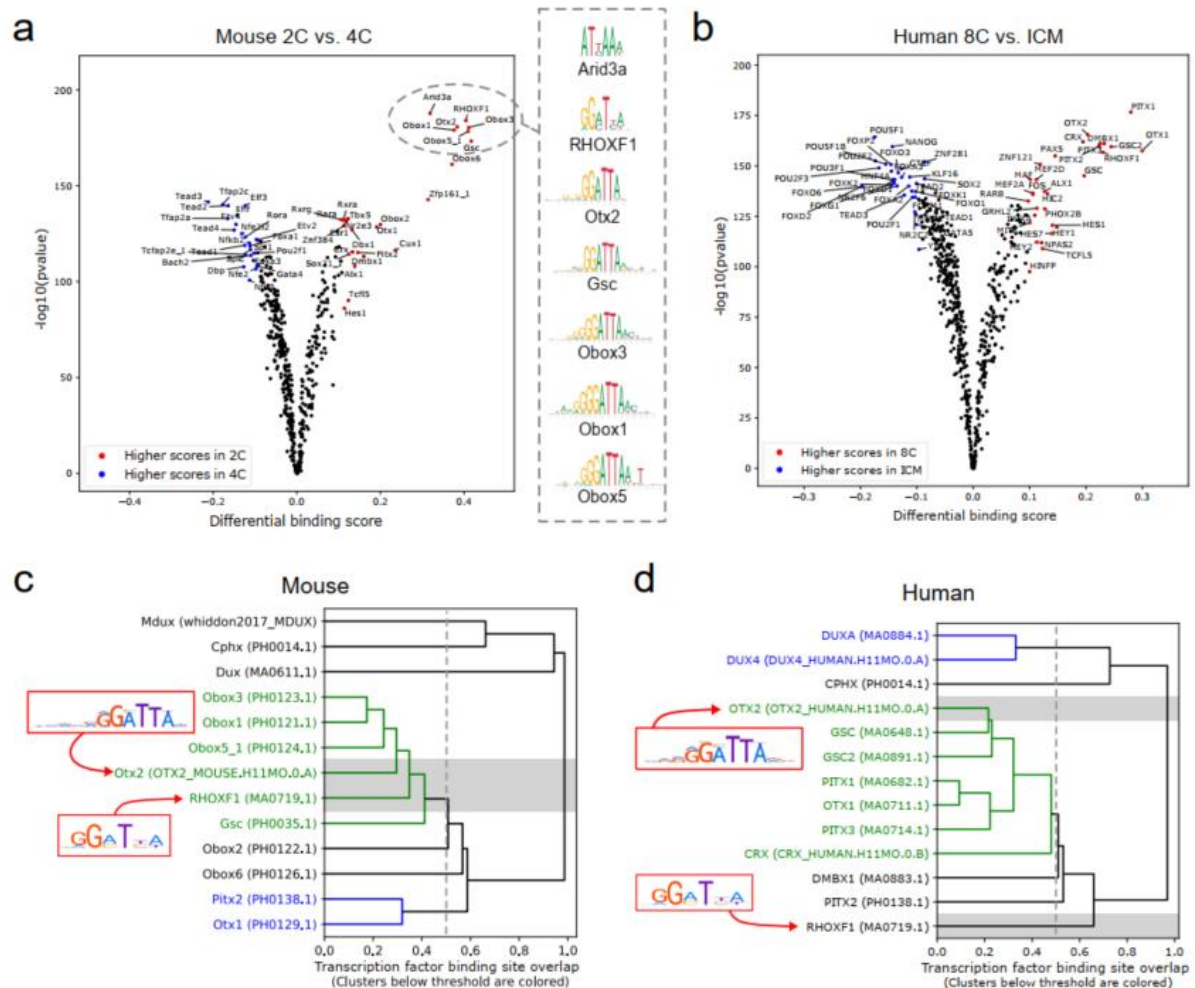
724 **Figure 2: TOBIAS enables investigation of global changes in transcription factor**

725 **binding**

726 **(a) Clustering of transcription factor activities throughout development.** Each row represents one
 727 TF, each column a developmental stage; blue color indicates low activity, red color indicates high
 728 activity. In order to visualize cluster trends, each cluster is associated with a trend line and time point
 729 specific boxplots.

730 **(b) Bias-corrected ATAC-seq footprints reveal dynamic TF binding.** Aggregated footprinting plot
 731 matrix for transcription factor binding sites. Plots are centered around binding motifs ($n=*$ relates to the
 732 number of binding sites). Rows indicate TFs DUX4, ZSCAN4, GATA2, and CTCF; columns illustrate
 733 developmental stages from left to right. Active binding of the individual TFs at the respective timepoints
 734 is visible as a depletion in the signal around the binding site (highlighted in red). Upper three TFs are
 735 related to developmental stages, CTCF acts as a universal control, generating a footprint in all
 736 conditions. See Supplementary Figure 2A for uncorrected footprints.

737 **(c) TF activity is shifted by ZGA onset in human and mouse.** Heatmaps show activity of known
738 ZGA-related TFs for human (left) and mouse (right) across matched timepoints 2C / 8C / ICM / hESC
739 (mESC). Mean TF activity (top panel) peaks at 4-8C stage in human and is shifted to 2-4C stage in
740 mouse by the earlier ZGA onset.
741



742

743 **Figure 3: Comparison of binding site overlaps shows specification of ZGA functions**
 744 **between mouse and human**

745 **(a-b) Pairwise comparison of TF activity between developmental stages.** The volcano plots show
 746 the differential binding activity against the $-\log_{10}(pvalue)$ (as provided by TOBIAS) of the investigated
 747 TF motifs; each dot represents one motif. For (A) 2C stage specific/significant TFs are labeled in red,
 748 4C specific factors are given in blue. For (B) 8C stage specific/significant TFs are labeled in red, ICM
 749 specific factors are given in blue.

750 **(c-d) Clustering of TF motifs based on binding site overlap.** Excerpt of the global TF clustering
 751 based on TF binding location, illustrating individual TFs as rows. The trees indicate genomic positional
 752 overlap of individual TFBS with a tree-depth of 0.2 representing an overlap of 80% of motifs. Each TF
 753 is indicated by name and unique ID in brackets. Clusters of TFs with more than 50% overlap (below 0.5
 754 tree distance) are colored. (C) shows overlap of motifs included in the mouse analysis, and (D) shows
 755 clustering of human motifs. Complete TF trees are provided in Supp. File 2 and Supp. File 3.

766 **(c) Change in expression of genes near Dux binding sites.** The heatmap shows 2664 Dux binding
767 sites found in gene promoters. Footprint $\log_2(FC)$ and RNA $\log_2(FC)$ represent the changes between
768 Control and DuxOE for footprints and gene expression, respectively. $\log_2(FC)$ is calculated as
769 $\log_2(\text{DuxOE}/\text{Control})$. The column "Binding prediction" depicts whether the binding site was predicted
770 by TOBIAS to be bound/unbound in the DuxOE condition.

771 **(d) Genomic tracks showing footprint scores of Dux-binding.** Genomic tracks indicating three DUX
772 target gene promoters (one per row) and respective tracks for cut site signals (red/blue), TOBIAS
773 footprints (blue), detected motifs (black boxes), and gene locations (solid black boxes with arrows
774 indicating gene strand).

775 **(e) Dux transcription factor network.** The TF-TF network is built of all TFBS with binding in TF
776 promoters with increasing strength in DuxOE ($\log_2(FC) > 0$). Sizes of nodes represent the level of the
777 network starting with Dux (Large: Dux, Medium: 1st level, Small: 2nd level). Nodes are colored based
778 on RNA level in the OE condition [5].

779 **(f) Correlation of the Dux transcription factor network to expression during development.** The
780 heatmap depicts the *in vivo* gene expression during developmental stages from [31]. The right-hand
781 group annotation highlights the difference in mean expression for each timepoint. The heatmap is split
782 into target genes of Dux, target genes of Arnt, Rxrg and Mef2d, as well as the pooled target genes from
783 Tbx4, Mafb, Zscan4c and Zscan4f (Additional targets).

784 **(g) Dux binding sites overlap with repeat elements.** All potential Dux binding sites are split into sites
785 either overlapping promoters/genes or without annotation to any known genes. The bottom pie chart
786 shows a subset of the latter, additionally having highly increased binding ($\log_2(FC) > 1$), and overlapping
787 LTR/LINE1 elements.

788 **(h) Dux induces expression of transcripts specific for preimplantation.** Genomic signals for the
789 Dux binding sites which are bound in DuxOE with $\log_2(FC)$ footprint score > 1 (i.e. upregulated in
790 DuxOE) are split into overlapping either LTR, LINE1 or no known genetic elements (top to bottom).
791 Footprint scores ($\pm 100\text{bp}$ from Dux binding sites) indicate the differential Dux binding between control
792 and DuxOE. RNA-seq shows the normalized read-counts from [5] and [31] within $\pm 5\text{kb}$ of the
793 respective Dux binding sites, while red color indicates high expression.

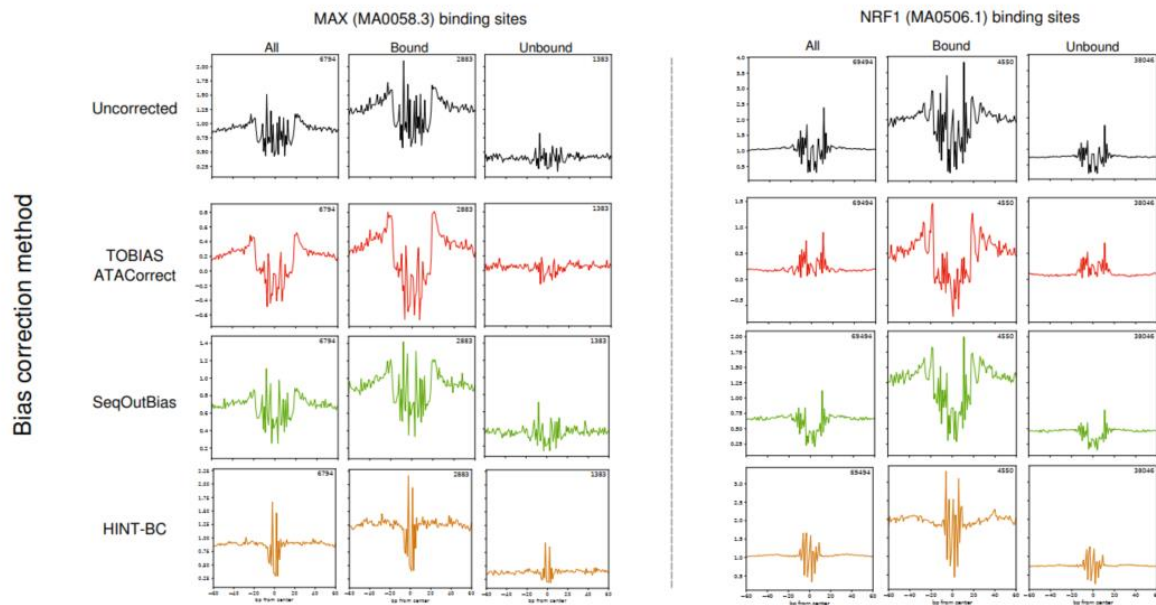
794

795

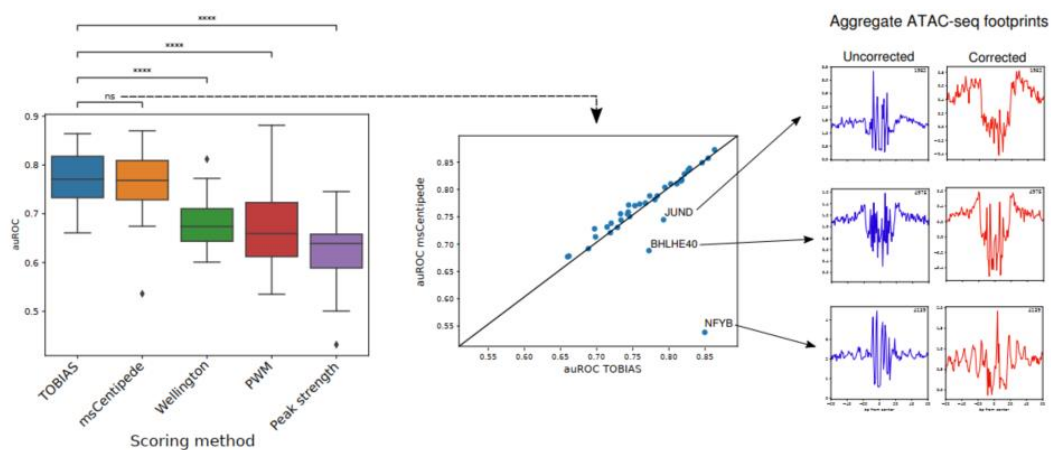
796

797

a Comparison of bias-correction methods



b Comparison of footprinting methods

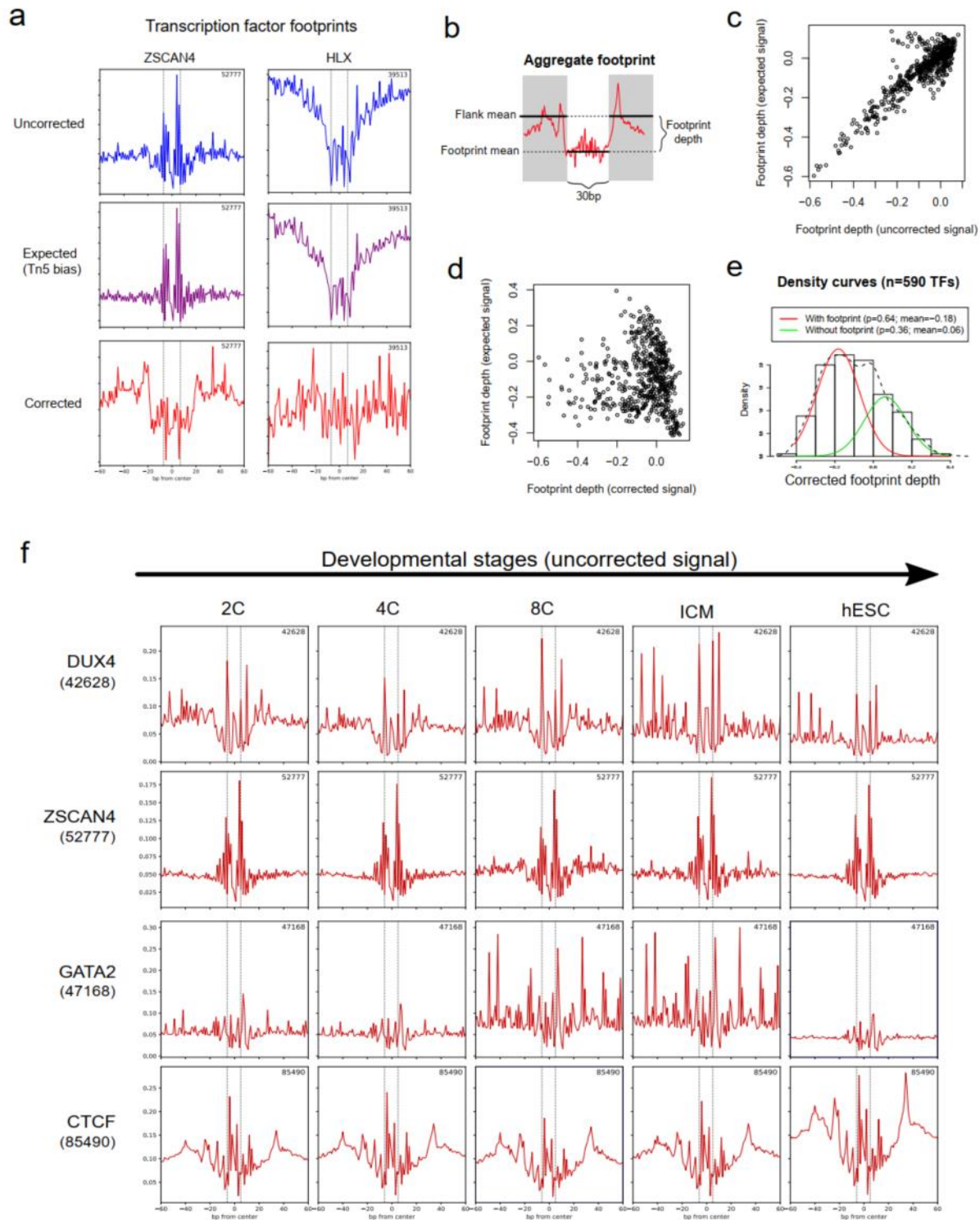


798

799 **Supplementary Figure 1: Comparison of existing bias-correction and footprinting**
 800 **methods**

801 **(a) Comparison of aggregate footprints for different bias-correction methods.** Bound and
 802 unbound transcription factor binding sites for MAX and NRF1 are shown across uncorrected signal
 803 (pileup of Tn5 insertions), TOBIAS ATACCorrect, SeqOutBias and HINT-BC correction methods. An
 804 overview of all included TFs can be found in Supplementary File 1.

805 **(b) Comparison of predictive ability across different footprinting methods.** (left) auROC is
806 calculated based on ENCODE ChIP-seq for 36 TFs and compared across methods. Boxes indicate
807 quantiles, horizontal line indicates mean auROC of all TFs. Significance is indicated if applicable as
808 asterisk. (center) TOBIAS and msCentipede are compared by pairwise dotplot, each dot represents
809 one TF, TOBIAS has significant gains in auROC for JUND, BHLHE40 and NFYB, for which individual
810 aggregated footprints are shown (left, uncorrected in blue, corrected in red)
811



812

813 **Supplementary Figure 2: Tn5-bias correction is important for visualization of**

814 **footprints from ATAC-seq**

815 *(a) Examples of Tn5-bias correction using “expected”-intermediates. For ZSCAN4, the*

816 *uncorrected signal is clearly influenced by the expected Tn5 bias, whereas the corrected signal*

817 *uncovers the underlying effect of protein binding. Likewise, the uncorrected signal of HLX resembles a*
818 *footprint which is mirrored by the expected signal. However, the corrected signal shows uniformity and*
819 *uncovers that there is little effect of protein binding.*

820 **(b) Aggregate footprint depth model.** *The footprint depth is calculated using a similar metric as*
821 *described in [22].*

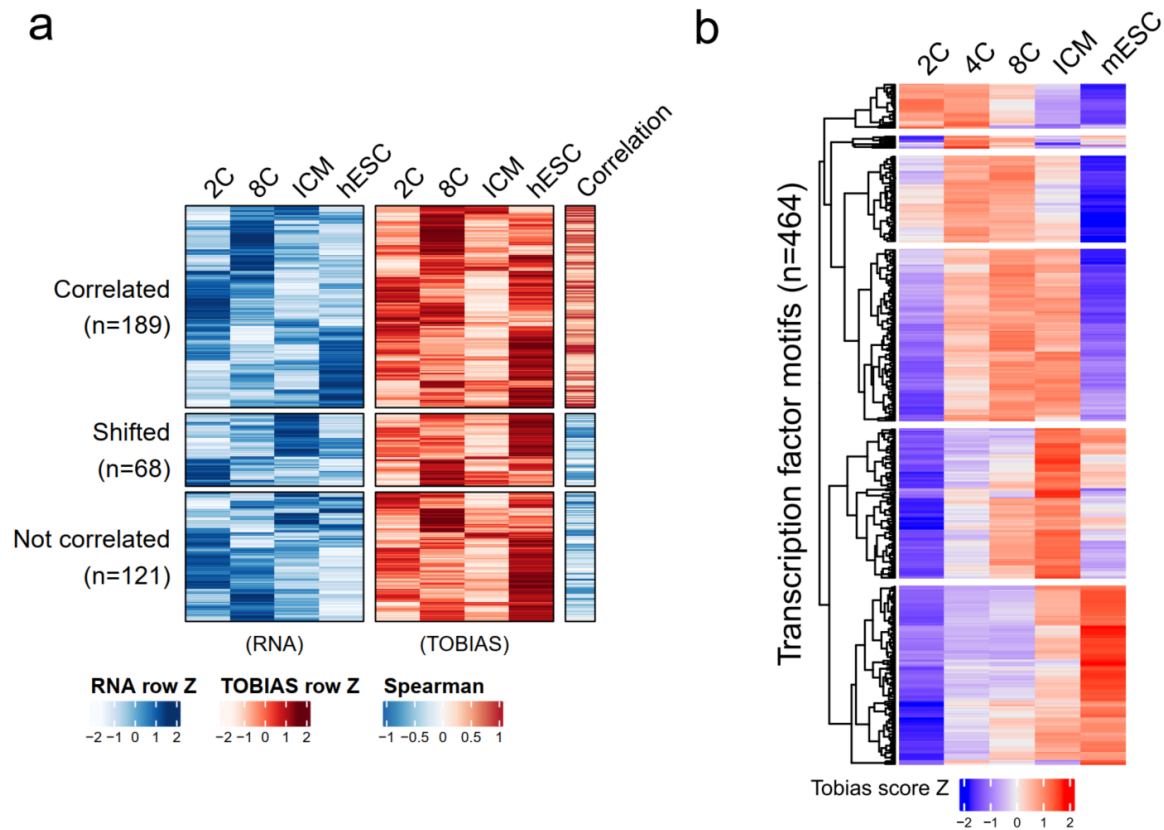
822 **(c) Uncorrected Tn5-bias.** *The scatter plot show the depth of footprints for uncorrected vs. expected*
823 *footprints*

824 **(d) Corrected Tn5-bias. The scatter plot** *show the depth of corrected vs. expected footprints.*

825 **(e) Mixture model** *of all footprinting depths shows that 65% of motifs fall into the category of a*
826 *measurable footprint in the aggregated profile. Data is based on 590 motifs in hESC.*

827 **(f) A depiction of uncorrected footprint aggregates across timepoints for transcription factors**
828 **DUX4, ZSCAN4, GATA2 and CTCF.** *In contrast to the corresponding corrected signals seen in Figure*
829 *2A, the footprints are hardly visible in the uncorrected aggregates.*

830



831

832 **Supplementary Figure 3: Transcription factor activity and expression during mouse and**
 833 **human development**

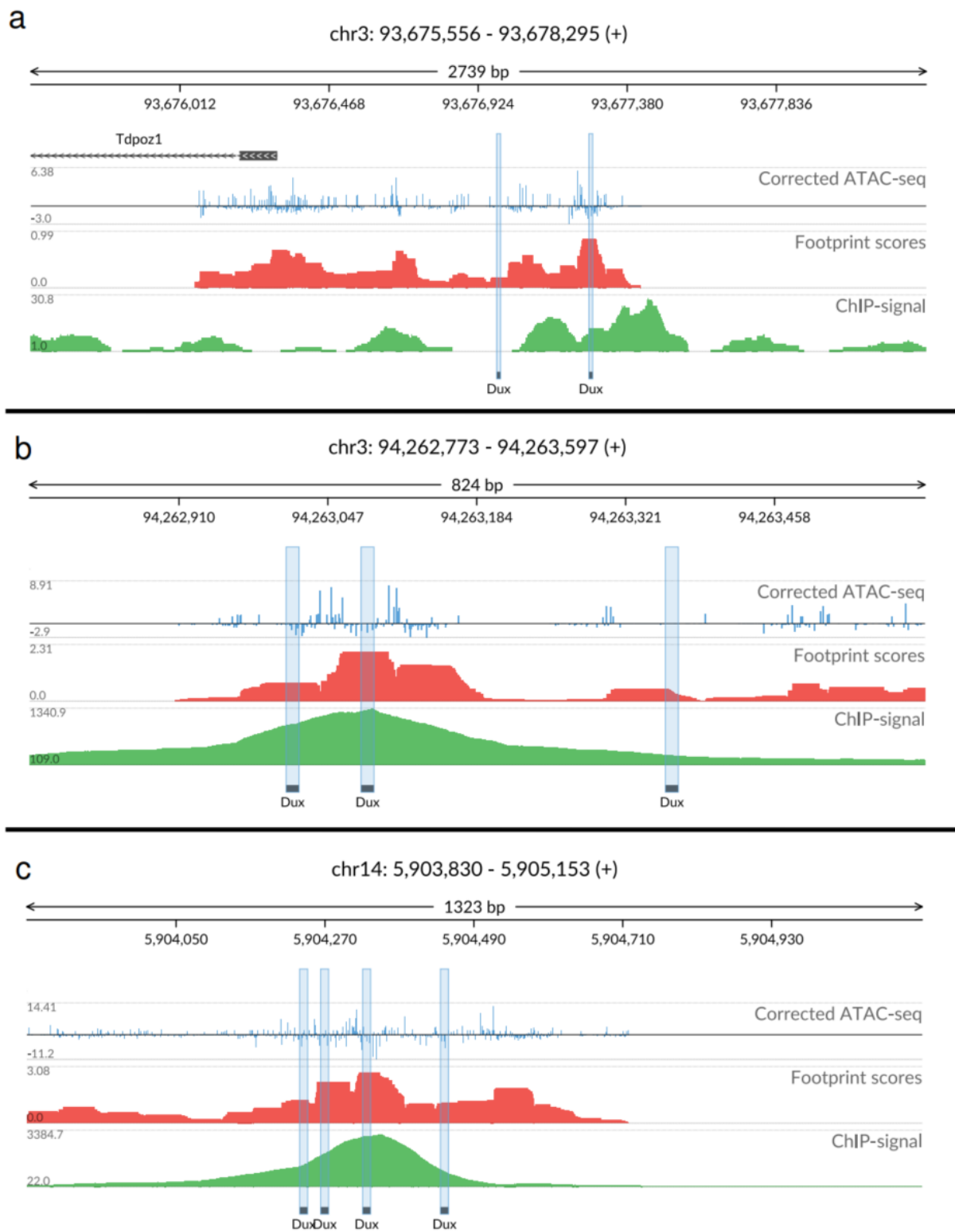
834 **(a) Correlation of footprints and RNA-seq.** The left heatmap (blue) depicts expression of transcription
 835 factor clusters in the respective developmental stages. The left heatmap (red) depicts the corresponding
 836 TOBIAS scores across human developmental stages. Spearman column represents the spearman
 837 correlation between TOBIAS/RNA. The TF clusters are grouped into “Correlated” (Spearman \geq 0.2),
 838 “shifted” (RNA max value appears before TOBIAS max value) and “Not correlated” (Spearman $<$ 0.2 with
 839 no apparent shift in RNA).

840 **(b) Dynamic transcription factor binding during mouse embryonic development.** Similarly to
 841 figure 2A, the heatmap depicts the TOBIAS-predicted footprint scores for 464 motifs during the
 842 timepoints 2C, 4C, 8C, ICM and mESC. The rows are clustered into 6 clusters using hierarchical
 843 clustering. Individual cluster members are given in Supplementary Table 2.

844

845

846



847

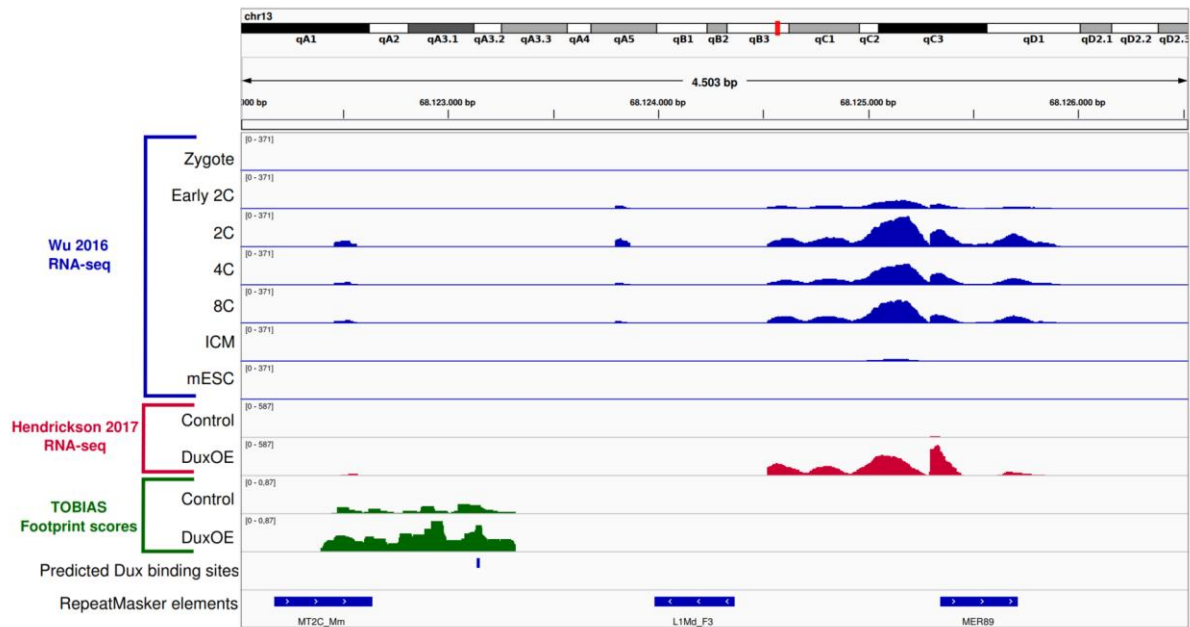
848 **Supplementary Figure 4: Predicted footprinting scores correlate with ChIP-signal for**

849 **Dux**

850 **(a) A view of the footprinting scores in the promoter of *Tdpoz1*.** Genomic tracks show corrected
851 ATAC-seq cutsites at 1bp resolution (blue), footprint scores as calculated by TOBIAS (red), and pileup
852 of reads from Dux ChIP-seq of [5] (green). Potential Dux binding sites are highlighted in blue.

853 **(b-c) Footprinting correlates with ChIP-signal at multiple genomic loci.** Genomic tracks are the
854 same as described for (a).

855



856
857

858 **Supplementary Figure 5: Predicted Dux binding site correlates with increase in**
859 **expression of closely non-annotated regions**

860 *The figure shows genomic tracks of RNA-seq from [31] (blue) and [5] (red), TOBIAS footprint scores*
861 *predicted from ATAC-seq (green) ([5]), predicted Dux binding site as well as known repeats as*
862 *annotated by RepeatMasker (Smit, AFA, Hubley, R & Green, P. RepeatMasker Open-4.0).*

863

864 **Supplemental Information**

865 List of Supplementary Files

866 *Supplementary File 1: Visualization of different methods for Tn5 bias correction across all 36*
867 *TFs with matched ChIP-seq. Each page contains footprints for a specific TF across all binding*
868 *sites (in peaks), bound sites (overlapping ChIP-seq) and unbound sites (not overlapping ChIP-*
869 *seq) for uncorrected/expected/corrected signals from different bias correction methods.*

870 *Supplementary File 2: The direct output file of the “TOBIAS BINDetect”-module containing*
871 *differential binding plots across all pairwise-comparisons of human developmental stages.*

872 *Supplementary File 3: The direct output file of the “TOBIAS BINDetect”-module containing*
873 *differential binding plots across all pairwise-comparisons of mouse developmental stages.*

874 *Supplementary File 4: The direct output file of the “TOBIAS BINDetect”-module containing*
875 *differential binding plots between control (mESC) and DuxOE samples.*

876

877 List of Supplementary Tables

878 *Supplementary Table 1: Prediction of transcription factor binding across human*
879 *2C/4C/8C/ICM/hESC clustered into co-active TFs. Each transcription factor is further linked to*
880 *expression of the factor based on RNA-seq.*

881 *Supplementary Table 2: TOBIAS TF scores for human PD timepoints, correlated to*
882 *corresponding RNA expression.*

883 *Supplementary Table 3: Prediction of transcription factor binding across mouse*
884 *2C/4C/8C/ICM/mESC clustered into co-active TFs. Each transcription factor is further linked*
885 *to expression of the factor based on RNA-seq.*

886 *Supplementary Table 4: Human and Mouse RNA expression for Obox and RHOX/Rhox genes*
887 *during preimplantation developmental stages.*

888 *Supplementary Table 5: Full list of the predicted Dux binding sites as well as their change*
889 *between mESC and DuxOE as predicted by TOBIAS.*

890

891 References

892

- 893 1. Buenrostro JD, Giresi PG, Zaba LC, Chang HY, Greenleaf WJ: **Transposition of**
894 **native chromatin for fast and sensitive epigenomic profiling of open chromatin,**
895 **DNA-binding proteins and nucleosome position.** *Nat Methods* 2013, **10**:1213-
896 1218.
- 897 2. Skene PJ, Henikoff S: **An efficient targeted nuclease strategy for high-resolution**
898 **mapping of DNA binding sites.** *eLife* 2017, **6**:e21856.
- 899 3. Eckersley-Maslin MA, Alda-Catalinas C, Reik W: **Dynamics of the epigenetic**
900 **landscape during the maternal-to-zygotic transition.** *Nat Rev Mol Cell Biol* 2018,
901 **19**:436-450.
- 902 4. Jukam D, Shariati SAM, Skotheim JM: **Zygotic Genome Activation in Vertebrates.**
903 *Dev Cell* 2017, **42**:316-332.
- 904 5. Hendrickson PG, Dorais JA, Grow EJ, Whiddon JL, Lim JW, Wike CL, Weaver BD,
905 Pflueger C, Emery BR, Wilcox AL, et al: **Conserved roles of mouse DUX and human**
906 **DUX4 in activating cleavage-stage genes and MERVL/HERVL retrotransposons.**
907 *Nat Genet* 2017, **49**:925-934.
- 908 6. De Iaco A, Planet E, Coluccio A, Verp S, Duc J, Trono D: **DUX-family transcription**
909 **factors regulate zygotic genome activation in placental mammals.** *Nat Genet*
910 2017, **49**:941-945.
- 911 7. Eckersley-Maslin MA, Svensson V, Krueger C, Stubbs TM, Giehr P, Krueger F,
912 Miragaia RJ, Kyriakopoulos C, Berrens RV, Milagre I, et al: **MERVL/Zscan4 Network**
913 **Activation Results in Transient Genome-wide DNA Demethylation of mESCs.**
914 *Cell Rep* 2016, **17**:179-192.
- 915 8. Madisson E, Jouhilahti EM, Vesterlund L, Tohonen V, Krjutskov K, Petropoulos S,
916 Einarsdottir E, Linnarsson S, Lanner F, Mansson R, et al: **Characterization and target**
917 **genes of nine human PRD-like homeobox domain genes expressed exclusively**
918 **in early embryos.** *Sci Rep* 2016, **6**:28995.
- 919 9. Hesselberth JR, Chen X, Zhang Z, Sabo PJ, Sandstrom R, Reynolds AP, Thurman
920 RE, Neph S, Kuehn MS, Noble WS, et al: **Global mapping of protein-DNA**
921 **interactions in vivo by digital genomic footprinting.** *Nat Methods* 2009, **6**:283-289.
- 922 10. Galas DJ, Schmitz A: **DNase footprinting: a simple method for the detection of**
923 **protein-DNA binding specificity.** *Nucleic Acids Res* 1978, **5**:3157-3170.
- 924 11. Sung MH, Baek S, Hager GL: **Genome-wide footprinting: ready for prime time?**
925 *Nat Methods* 2016, **13**:222-228.
- 926 12. Vierstra J, Stamatoyannopoulos JA: **Genomic footprinting.** *Nat Methods* 2016,
927 **13**:213-221.
- 928 13. Quach B, Furey TS: **DeFCoM: analysis and modeling of transcription factor**
929 **binding sites using a motif-centric genomic footprinter.** *Bioinformatics* 2017,
930 **33**:956-963.
- 931 14. Raj A, Shim H, Gilad Y, Pritchard JK, Stephens M: **msCentipede: Modeling**
932 **Heterogeneity across Genomic Sites and Replicates Improves Accuracy in the**
933 **Inference of Transcription Factor Binding.** *PLoS One* 2015, **10**:e0138030.
- 934 15. Chen X, Yu B, Carriero N, Silva C, Bonneau R: **Mocap: large-scale inference of**
935 **transcription factor binding sites from chromatin accessibility.** *Nucleic Acids Res*
936 2017, **45**:4315-4329.
- 937 16. Li Z, Schulz MH, Look T, Begemann M, Zenke M, Costa IG: **Identification of**
938 **transcription factor binding sites using ATAC-seq.** *Genome biology* 2019, **20**:45-
939 45.
- 940 17. Koohy H, Down TA, Hubbard TJ: **Chromatin accessibility data sets show bias due**
941 **to sequence specificity of the DNase I enzyme.** *PLoS One* 2013, **8**:e69853.
- 942 18. Sung MH, Guertin MJ, Baek S, Hager GL: **DNase footprint signatures are dictated**
943 **by factor dynamics and DNA sequence.** *Mol Cell* 2014, **56**:275-285.

- 944 19. He HH, Meyer CA, Hu SS, Chen MW, Zang C, Liu Y, Rao PK, Fei T, Xu H, Long H, et
945 al: **Refined DNase-seq protocol and data analysis reveals intrinsic bias in**
946 **transcription factor footprint identification.** *Nat Methods* 2014, **11**:73-78.
- 947 20. Madrigal P: **On Accounting for Sequence-Specific Bias in Genome-Wide**
948 **Chromatin Accessibility Experiments: Recent Advances and Contradictions.**
949 *Front Bioeng Biotechnol* 2015, **3**:144.
- 950 21. Tripodi IJ, Allen MA, Dowell RD: **Detecting Differential Transcription Factor Activity**
951 **from ATAC-Seq Data.** *Molecules* 2018, **23**.
- 952 22. Baek S, Goldstein I, Hager GL: **Bivariate Genomic Footprinting Detects Changes**
953 **in Transcription Factor Activity.** *Cell Rep* 2017, **19**:1710-1722.
- 954 23. Berest I, Arnold C, Reyes-Palomares A, Palla G, Rasmussen KD, Helin K, Zaugg JB:
955 **Quantification of differential transcription factor activity and multiomics-based**
956 **classification into activators and repressors: diffTF.**
957 *bioRxiv* 2018:368498.
- 958 24. Gusmao EG, Allhoff M, Zenke M, Costa IG: **Analysis of computational footprinting**
959 **methods for DNase sequencing experiments.** *Nat Methods* 2016, **13**:303-309.
- 960 25. Martins AL, Walavalkar NM, Anderson WD, Zang C, Guertin MJ: **Universal correction**
961 **of enzymatic sequence bias reveals molecular signatures of protein/DNA**
962 **interactions.** *Nucleic Acids Res* 2018, **46**:e9.
- 963 26. Wang JR, Quach B, Furey TS: **Correcting nucleotide-specific biases in high-**
964 **throughput sequencing data.** *BMC Bioinformatics* 2017, **18**:357.
- 965 27. Koster J, Rahmann S: **Snakemake-a scalable bioinformatics workflow engine.**
966 *Bioinformatics* 2018, **34**:3600.
- 967 28. Di Tommaso P, Chatzou M, Floden EW, Barja PP, Palumbo E, Notredame C:
968 **Nextflow enables reproducible computational workflows.** *Nat Biotechnol* 2017,
969 **35**:316-319.
- 970 29. Belmann P, Fischer B, Krüger J, Procházka M, Rasche H, Prinz M, Hanussek M, Lang
971 M, Bartusch F, Gläßle B, et al: **de.NBI Cloud federation through ELIXIR AAI**
972 **[version 1; peer review: 2 approved, 1 not approved].** *F1000Research* 2019, **8**.
- 973 30. Wu J, Xu J, Liu B, Yao G, Wang P, Lin Z, Huang B, Wang X, Li T, Shi S, et al:
974 **Chromatin analysis in human early development reveals epigenetic transition**
975 **during ZGA.** *Nature* 2018, **557**:256-260.
- 976 31. Wu J, Huang B, Chen H, Yin Q, Liu Y, Xiang Y, Zhang B, Liu B, Wang Q, Xia W, et al:
977 **The landscape of accessible chromatin in mammalian preimplantation embryos.**
978 *Nature* 2016, **534**:652-657.
- 979 32. Wang K, Nishida H: **REGULATOR: a database of metazoan transcription factors**
980 **and maternal factors for developmental studies.** *BMC Bioinformatics* 2015, **16**:114.
- 981 33. Adjaye J, Monk M: **Transcription of homeobox-containing genes detected in**
982 **cDNA libraries derived from human unfertilized oocytes and preimplantation**
983 **embryos.** *Mol Hum Reprod* 2000, **6**:707-711.
- 984 34. Adhikary S, Peukert K, Karsunky H, Beuger V, Lutz W, Elsasser HP, Moroy T, Eilers
985 M: **Miz1 is required for early embryonic development during gastrulation.** *Mol*
986 *Cell Biol* 2003, **23**:7648-7657.
- 987 35. Home P, Kumar RP, Ganguly A, Saha B, Milano-Foster J, Bhattacharya B, Ray S,
988 Gunewardena S, Paul A, Camper SA, et al: **Genetic redundancy of GATA factors**
989 **in the extraembryonic trophoblast lineage ensures the progression of**
990 **preimplantation and postimplantation mammalian development.** *Development*
991 2017, **144**:876-888.
- 992 36. Xu K, Chen X, Yang H, Xu Y, He Y, Wang C, Huang H, Liu B, Liu W, Li J, et al:
993 **Maternal Sall4 Is Indispensable for Epigenetic Maturation of Mouse Oocytes.**
994 *Journal of Biological Chemistry* 2017, **292**:1798-1807.
- 995 37. Svoboda P: **Mammalian zygotic genome activation.** *Semin Cell Dev Biol* 2018,
996 **84**:118-126.
- 997 38. Schulz KN, Harrison MM: **Mechanisms regulating zygotic genome activation.**
998 *Nature Reviews Genetics* 2019, **20**:221-234.

- 999 39. Tohonen V, Katayama S, Vesterlund L, Jouhilahti EM, Sheikhi M, Madisson E,
1000 Filippini-Cattaneo G, Jaconi M, Johnsson A, Burglin TR, et al: **Novel PRD-like**
1001 **homeodomain transcription factors and retrotransposon elements in early**
1002 **human development.** *Nat Commun* 2015, **6**:8207.
- 1003 40. Rhee C, Edwards M, Dang C, Harris J, Brown M, Kim J, Tucker HO: **ARID3A is**
1004 **required for mammalian placenta development.** *Developmental Biology* 2017,
1005 **422**:83-91.
- 1006 41. Winger Q, Huang J, Auman HJ, Lewandoski M, Williams T: **Analysis of Transcription**
1007 **Factor AP-2 Expression and Function During Mouse Preimplantation**
1008 **Development1.** *Biology of Reproduction* 2006, **75**:324-333.
- 1009 42. Pastor WA, Liu W, Chen D, Ho J, Kim R, Hunt TJ, Lukianchikov A, Liu X, Polo JM,
1010 Jacobsen SE, Clark AT: **TFAP2C regulates transcription in human naive**
1011 **pluripotency by opening enhancers.** *Nat Cell Biol* 2018, **20**:553-564.
- 1012 43. Eckersley-Maslin M, Alda-Catalinas C, Blotenburg M, Kreibich E, Krueger C, Reik W:
1013 **Dppa2 and Dppa4 directly regulate the Dux-driven zygotic transcriptional**
1014 **program.** *Genes Dev* 2019, **33**:194-208.
- 1015 44. De Iaco A, Coudray A, Duc J, Trono D: **DPPA2 and DPPA4 are necessary to**
1016 **establish a 2C-like state in mouse embryonic stem cells.** *EMBO Rep* 2019, **20**.
- 1017 45. Whiddon JL, Langford AT, Wong CJ, Zhong JW, Tapscott SJ: **Conservation and**
1018 **innovation in the DUX4-family gene network.** *Nat Genet* 2017, **49**:935-940.
- 1019 46. Huang CJ, Chen CY, Chen HH, Tsai SF, Choo KB: **TDPOZ, a family of bipartite**
1020 **animal and plant proteins that contain the TRAF (TD) and POZ/BTB domains.**
1021 *Gene* 2004, **324**:117-127.
- 1022 47. Lee S-E, Lee S-Y, Lee K-A: **Rhox in mammalian reproduction and development.**
1023 *Clin Exp Reprod Med* 2013, **40**:107-114.
- 1024 48. Borgmann J, Tuttelmann F, Dworniczak B, Ropke A, Song HW, Kliesch S, Wilkinson
1025 MF, Laurentino S, Gromoll J: **The human RHOX gene cluster: target genes and**
1026 **functional analysis of gene variants in infertile men.** *Hum Mol Genet* 2016,
1027 **25**:4898-4910.
- 1028 49. Royall AH, Maeso I, Dunwell TL, Holland PWH: **Mouse Obox and Crxos modulate**
1029 **preimplantation transcriptional profiles revealing similarity between paralogous**
1030 **mouse and human homeobox genes.** *Evodevo* 2018, **9**:2.
- 1031 50. Percharde M, Lin CJ, Yin Y, Guan J, Peixoto GA, Bulut-Karslioglu A, Biechele S,
1032 Huang B, Shen X, Ramalho-Santos M: **A LINE1-Nucleolin Partnership Regulates**
1033 **Early Development and ESC Identity.** *Cell* 2018, **174**:391-405.e319.
- 1034 51. Buenrostro JD, Wu B, Litzenburger UM, Ruff D, Gonzales ML, Snyder MP, Chang HY,
1035 Greenleaf WJ: **Single-cell chromatin accessibility reveals principles of regulatory**
1036 **variation.** *Nature* 2015, **523**:486-490.
- 1037 52. Harrison PW, Alako B, Amid C, Cerdeno-Tarraga A, Cleland I, Holt S, Hussein A,
1038 Jayathilaka S, Kay S, Keane T, et al: **The European Nucleotide Archive in 2018.**
1039 *Nucleic Acids Res* 2018.
- 1040 53. Martin M: **Cutadapt removes adapter sequences from high-throughput**
1041 **sequencing reads.** *2011* 2011, **17**:3.
- 1042 54. Dobin A, Davis CA, Schlesinger F, Drenkow J, Zaleski C, Jha S, Batut P, Chaisson M,
1043 Gingeras TR: **STAR: ultrafast universal RNA-seq aligner.** *Bioinformatics* 2013,
1044 **29**:15-21.
- 1045 55. Zerbino DR, Achuthan P, Akanni W, Amode MR, Barrell D, Bhai J, Billis K, Cummins
1046 C, Gall A, Giron CG, et al: **Ensembl 2018.** *Nucleic Acids Res* 2018, **46**:D754-D761.
- 1047 56. Feng JX, Liu T, Qin B, Zhang Y, Liu XS: **Identifying ChIP-seq enrichment using**
1048 **MACS.** *Nature Protocols* 2012, **7**:1728-1740.
- 1049 57. Frankish A, Diekhans M, Ferreira A-M, Johnson R, Jungreis I, Loveland J, Mudge JM,
1050 Sisu C, Wright J, Armstrong J, et al: **GENCODE reference annotation for the human**
1051 **and mouse genomes.** *Nucleic Acids Research* 2018, **47**:D766-D773.
- 1052 58. Kondili M, Fust A, Preussner J, Kuenne C, Braun T, Looso M: **UROPA: a tool for**
1053 **Universal ROBust Peak Annotation.** *Sci Rep* 2017, **7**:2593.

- 1054 59. Love MI, Huber W, Anders S: **Moderated estimation of fold change and dispersion**
1055 **for RNA-seq data with DESeq2.** *Genome biology* 2014, **15**:550-550.
- 1056 60. Bolger AM, Lohse M, Usadel B: **Trimmomatic: a flexible trimmer for Illumina**
1057 **sequence data.** *Bioinformatics* 2014, **30**:2114-2120.
- 1058 61. Khan A, Fornes O, Stigliani A, Gheorghe M, Castro-Mondragon JA, van der Lee R,
1059 Bessy A, Cheneby J, Kulkarni SR, Tan G, et al: **JASPAR 2018: update of the open-**
1060 **access database of transcription factor binding profiles and its web framework.**
1061 *Nucleic Acids Res* 2018, **46**:D1284.
- 1062 62. Kulakovskiy IV, Vorontsov IE, Yevshin IS, Sharipov RN, Fedorova AD, Rumynskiy EI,
1063 Medvedeva YA, Magana-Mora A, Bajic VB, Papatsenko DA, et al: **HOCOMOCO:**
1064 **towards a complete collection of transcription factor binding models for human**
1065 **and mouse via large-scale ChIP-Seq analysis.** *Nucleic Acids Research* 2017,
1066 **46**:D252-D259.
- 1067 63. Sebastian A, Contreras-Moreira B: **footprintDB: a database of transcription factors**
1068 **with annotated cis elements and binding interfaces.** *Bioinformatics* 2013, **30**:258-
1069 265.
- 1070 64. Yin Y, Morgunova E, Jolma A, Kaasinen E, Sahu B, Khund-Sayeed S, Das PK, Kivioja
1071 T, Dave K, Zhong F, et al: **Impact of cytosine methylation on DNA binding**
1072 **specificities of human transcription factors.** *Science* 2017, **356**:eaaj2239.
- 1073 65. Machanick P, Bailey TL: **MEME-CHIP: motif analysis of large DNA datasets.**
1074 *Bioinformatics* 2011, **27**:1696-1697.
- 1075 66. Durinck S, Spellman PT, Birney E, Huber W: **Mapping identifiers for the integration**
1076 **of genomic datasets with the R/Bioconductor package biomaRt.** *Nature Protocols*
1077 2009, **4**:1184.
- 1078 67. Gu L, Hitzel J, Moll F, Kruse C, Malik RA, Preussner J, Looso M, Leisegang MS,
1079 Steinhilber D, Brandes RP, Fork C: **The Histone Demethylase PHF8 Is Essential for**
1080 **Endothelial Cell Migration.** *PLoS One* 2016, **11**:e0146645.
- 1081 68. Robinson JT, Thorvaldsdóttir H, Winckler W, Guttman M, Lander ES, Getz G, Mesirov
1082 JP: **Integrative genomics viewer.** *Nature biotechnology* 2011, **29**:24-26.
- 1083 69. Egorov AA, Sakharova EA, Anisimova AS, Dmitriev SE, Gladyshev VN, Kulakovskiy
1084 IV: **svist4get: a simple visualization tool for genomic tracks from sequencing**
1085 **experiments.** *BMC Bioinformatics* 2019, **20**:113.
- 1086 70. Shannon P, Markiel A, Ozier O, Baliga NS, Wang JT, Ramage D, Amin N, Schwikowski
1087 B, Ideker T: **Cytoscape: A Software Environment for Integrated Models of**
1088 **Biomolecular Interaction Networks.** *Genome Research* 2003, **13**:2498-2504.
- 1089 71. Ramírez F, Ryan DP, Grüning B, Bhardwaj V, Kilpert F, Richter AS, Heyne S, Dündar
1090 F, Manke T: **deepTools2: a next generation web server for deep-sequencing data**
1091 **analysis.** *Nucleic acids research* 2016, **44**:W160-W165.
- 1092 72. Siddharthan R: **Dinucleotide weight matrices for predicting transcription factor**
1093 **binding sites: generalizing the position weight matrix.** *PLoS One* 2010, **5**:e9722.
- 1094 73. Korhonen JH, Palin K, Taipale J, Ukkonen E: **Fast motif matching revisited: high-**
1095 **order PWMs, SNPs and indels.** *Bioinformatics* 2016, **33**:514-521.
- 1096 74. Benaglia T, Chauveau D, Hunter DR, Young DS: **mixtools: An R Package for**
1097 **Analyzing Mixture Models.** *Journal of Statistical Software; Vol 1, Issue 6 (2010)* 2009.
- 1098 75. Neph S, Vierstra J, Stergachis AB, Reynolds AP, Haugen E, Vernot B, Thurman RE,
1099 John S, Sandstrom R, Johnson AK, et al: **An expansive human regulatory lexicon**
1100 **encoded in transcription factor footprints.** *Nature* 2012, **489**:83-90.
- 1101 76. Piper J, Elze MC, Cauchy P, Cockerill PN, Bonifer C, Ott S: **Wellington: a novel**
1102 **method for the accurate identification of digital genomic footprints from DNase-**
1103 **seq data.** *Nucleic Acids Res* 2013, **41**:e201.
- 1104 77. Boyle AP, Song L, Lee BK, London D, Keefe D, Birney E, Iyer VR, Crawford GE, Furey
1105 TS: **High-resolution genome-wide in vivo footprinting of diverse transcription**
1106 **factors in human cells.** *Genome Res* 2011, **21**:456-464.

- 1107 78. Pique-Regi R, Degner JF, Pai AA, Gaffney DJ, Gilad Y, Pritchard JK: **Accurate**
1108 **inference of transcription factor binding from DNA sequence and chromatin**
1109 **accessibility data.** *Genome Res* 2011, **21**:447-455.
- 1110 79. Luo K, Hartemink AJ: **Using DNase digestion data to accurately identify**
1111 **transcription factor binding sites.** *Pac Symp Biocomput* 2013:80-91.
- 1112 80. Kahara J, Lahdesmaki H: **BinDNase: a discriminatory approach for transcription**
1113 **factor binding prediction using DNase I hypersensitivity data.** *Bioinformatics*
1114 2015, **31**:2852-2859.
- 1115 81. Bailey TL, Machanick P: **Inferring direct DNA binding from ChIP-seq.** *Nucleic Acids*
1116 *Research* 2012, **40**:e128-e128.
1117